AGU PUBLICATIONS

Global Biogeochemical Cycles

RESEARCH ARTICLE
10.1002/2017GB005700

Mercury in the Black Sea: New Insights From Measurements and Numerical Modeling

G. Rosati[1,2], L. E. Heimbürger[3], D. Melaku Canu[1], C. Lagane[4], L. Laffont[4], M. J. A. Rijkenberg[5], L. J. A. Gerringa[5], C. Solidoro[1,6], C. N. Gencarelli[7], I. M. Hedgecock[7], H. J. W. De Baar[5], and J. E. Sonke[4]

[1]OGS, National Institute of Oceanography and Experimental Geophysics, OCE Research Section, ECHO Group, Trieste, Italy, [2]Department of Life Sciences, University of Trieste, Trieste, Italy, [3]Aix Marseille Université, CNRS/INSU, Université de Toulon, IRD, Mediterranean Institute of Oceanography UM 110, Marseille, France, [4]Observatoire Midi-Pyrénées, Laboratoire Géosciences Environnement Toulouse, CNRS/IRD/Université Paul-Sabatier, Toulouse, France, [5]NIOZ, Royal Institute for Sea Research, department of GCO, Utrecht University, Den Burg, Netherlands, [6]ICTP, The Abdus Salam International Centre for Theoretical Physics, Trieste, Italy, [7]CNR, Institute of Atmospheric Pollution Research, Division of Rende, UNICAL-Polifunzionale, Rende, Italy

Abstract Redox conditions and organic matter control marine methylmercury (MeHg) production. The Black Sea is the world's largest and deepest anoxic basin and is thus ideal to study Hg species along the extended redox gradient. Here we present new dissolved Hg and MeHg data from the 2013 GEOTRACES MEDBlack cruise (GN04_leg2) that we integrated into a numerical 1-D model, to track the fate and dynamics of Hg and MeHg. Contrary to a previous study, our new data show highest MeHg concentrations in the permanently anoxic waters. Observed MeHg/Hg percentage (range 9–57%) in the anoxic waters is comparable to other subsurface maxima in oxic open-ocean waters. With the modeling we tested for various Hg methylation and demethylation scenarios along the redox gradient. The results show that Hg methylation must occur in the anoxic waters. The model was then used to simulate the time evolution (1850–2050) of Hg species in the Black Sea. Our findings quantify (1) inputs and outputs of Hg_T (~31 and ~28 kmol yr^{-1}) and $MeHg_T$ (~5 and ~4 kmol yr^{-1}) to the basin, (2) the extent of net demethylation occurring in oxic (~1 kmol yr^{-1}) and suboxic water (~6 kmol yr^{-1}), (3) and the net Hg methylation in the anoxic waters of the Black Sea (~11 kmol yr^{-1}). The model was also used to estimate the amount of anthropogenic Hg (85–93%) in the Black Sea.

Key Points:
- The 2013 GEOTRACES MEDBlack cruise data show the highest MeHg percentages (up to 57%) in permanently anoxic waters, comparable to oxic open-ocean subsurface maxima
- We implemented a 1-D numerical model for Hg dynamics and assessed the occurrence of Hg methylation and demethylation along the stretched redox gradient
- The Hg species model and budget suggest that input from rivers, the Mediterranean Sea, and sediment are negligible and that MeHg is produced in situ in anoxic waters

Supporting Information:
- Supporting Information S1
- Data Set S1
- Data Set S2

Correspondence to:
G. Rosati and L. E. Heimbürger,
grosati@ogs.trieste.it;
heimburger@lars-eric.com

Citation:
Rosati, G., Heimbürger, L. E., Melaku Canu, D., Lagane, C., Laffont, L., Rijkenberg, M. J. A., et al. (2018). Mercury in the Black Sea: New insights from measurements and numerical modeling. *Global Biogeochemical Cycles*, *32*, 529–550. https://doi.org/10.1002/2017GB005700

Received 22 APR 2017
Accepted 1 MAR 2018
Accepted article online 5 MAR 2018
Published online 13 APR 2018

1. Introduction

The ubiquitous presence of mercury (Hg) in the environment is a matter of concern due to the transformation of inorganic oxidized Hg (Hg^{II}) into methylmercury (MeHg), which is a biomagnifying neurotoxin (Clarkson & Magos, 2006; Cossa et al., 2012; Fitzgerald et al., 2007; Hammerschmidt & Fitzgerald, 2006). As humans are exposed to MeHg through fish consumption (Oken et al., 2012) understanding the mechanisms underlying MeHg production, degradation, transport, and accumulation in the marine environment is crucial.

Hg methylation is thought to be a primarily microbially driven process that occurs in marine sediments (Bouchet et al., 2013; Hammerschmidt et al., 2004; Hollweg et al., 2009, 2010; Monperrus, Tessier, Point, et al., 2007; Schartup et al., 2013) and the marine water column (Cossa et al., 2009; Heimbürger et al., 2010; Mason & Fitzgerald, 1990; Monperrus, Tessier, Point, et al., 2007; Monperrus, Tessier, Amouroux, et al., 2007; Sunderland et al., 2009) during remineralization of natural organic matter (NOM). NOM, which includes dissolved and particulate organic matter (i.e., DOM and POM, respectively), affects Hg methylation both acting as an electron donor for microbial activity and controlling Hg partitioning (Drott et al., 2007). Indeed, in the marine environment, Hg is effectively scavenged and transported by POM and also by authigenic Fe hydroxide and Mn oxide minerals (hereafter Fe/Mn oxides) and lithogenic particles (Lamborg et al., 2016). While sinking, particles undergo degradation, which prompts the release of dissolved Hg^{II} making it bioavailable to microbes (Cossa et al., 2009; Heimbürger et al., 2010; Muresan et al., 2007; Sunderland et al., 2009). Biogeochemical controls on Hg methylation rates are thus related both to the composition and the activity of the microbial community and to the speciation and partitioning of Hg^{II} (Cossa et al., 2014; Merritt & Amirbahman, 2009), with a critical role played by redox conditions, NOM availability, and quality (Bravo et al., 2017; Cossa et al., 2014; Schartup, Ndu, et al., 2015). Previous studies have used chemical equilibrium

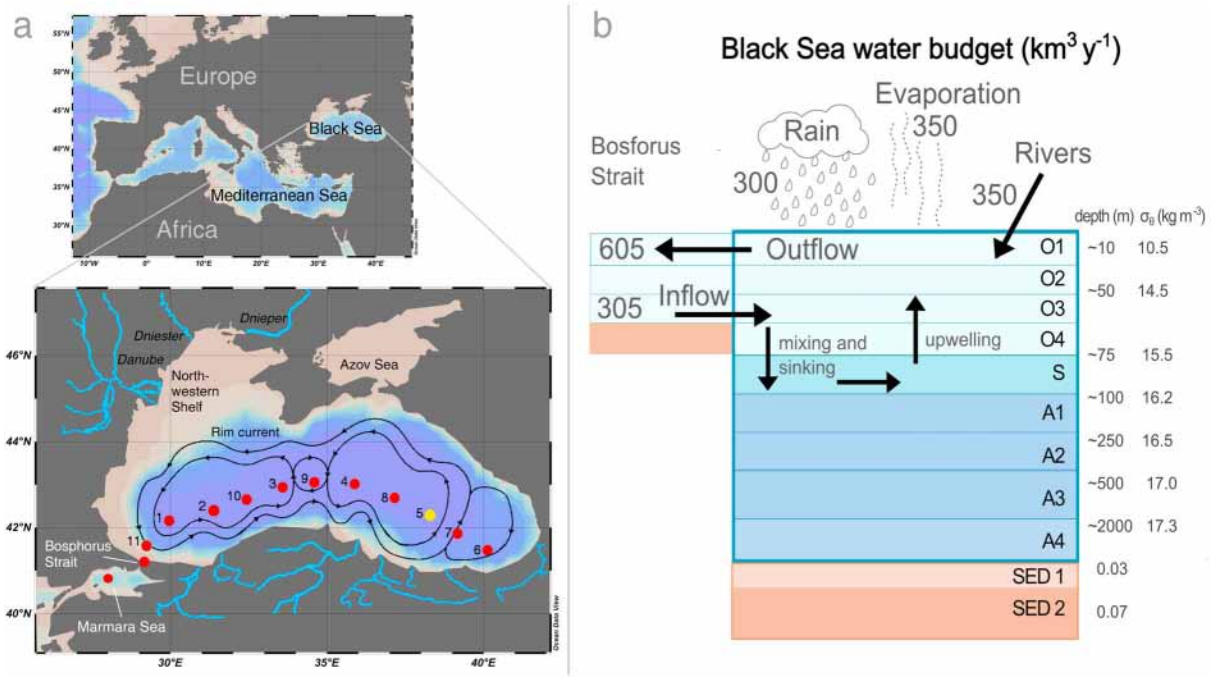

Figure 1. (a) The Black Sea with the 2013 GEOTRACES MedBlack cruise stations (red dots, the yellow dot indicates the position of the high-resolution profile). The Rim Current is shown in black lines. (b) Schematic description of the 1-D water budget for the Black Sea (after Özsoy & Ünlüata, 1997) as used in the model; sublayers are given on the right side (O1–O4 belong to the oxic layer, S is the suboxic layer, and A1–A4 belong to the anoxic layer).

modeling to explain the observed oxic or suboxic MeHg maxima in sediment and stratified water. These studies, which include a previous assessment of Hg species in the Black Sea water column, have concluded that methylation is hindered above sulfide concentrations of ~10 μM due to a shift of Hg speciation from neutral to charged species that makes it unavailable to microbes (Benoit, Gilmour, et al., 1999; Benoit, Mason, & Gilmour, 1999; Benoit et al., 2001; Lamborg et al., 2008). However, there is a lack of consensus on the relevance of the methylation process under different redox conditions. Hg methylation is known to be mediated by anaerobic bacteria (Gilmour et al., 2013); however, methylation in euxinic (i.e., anoxic and sulfidic) environments is not a well-understood process (Hsu-Kim et al., 2013; Merritt & Amirbahman, 2009), which has been shown to occur in sediments and lake water (Drott et al., 2007; Eckley & Hintelmann, 2006; Hollweg et al., 2009; King et al., 2000). The occurrence of Hg methylation in oxic waters was not discussed by Lamborg et al. (2008) for the Black Sea but has been shown to occur in other basins (Lehnherr et al., 2011; Monperrus, Tessier, Amouroux, et al., 2007; Schartup, Balcom, et al., 2015; Sharif et al., 2014). MeHg demethylation seems to occur at less variable rates among various environments, and the capacity of bacteria to demethylate seems to be more widespread (Heyes et al., 2006).

The Black Sea is ideal for investigating biogeochemical cycles under changing redox conditions because its waters encompass oxic, suboxic, and anoxic conditions (Schijf et al., 1991), with gradients stretched over several tens of meters. The Black Sea is a deep, semienclosed basin (Figure 1a, maps are plotted with Ocean Data View (Schlitzer, 2016), with permanently stratified water owing to the hydrological balance between the inflow of water from the Mediterranean Sea via the Marmara Sea-Bosporus system and freshwater inputs (Figure 1b and Text S1 in the supporting information) (Özsoy & Ünlüata, 1997). The surface circulation of the Black Sea is driven by two large cyclonic gyres in the eastern and western basin, which are connected to each other by the Rim Current that homogenizes surface waters (Murray et al., 2007). Vertical mixing is weak, and when oxygen depletion occurs, bacterial remineralization of NOM is driven by a sequence of alternative electron acceptors according to a sequence that is fixed across systems ($O_2 > N O_3^- > Mn_{Ox} > Fe_{Ox} > SO_4$) (Froelich et al., 1979). Hence, the redox progression along the Black Sea water column is similar to the one in sedimentary environments and hypoxic basins worldwide, with the advantage that the redox layers of the Black Sea are quite stable throughout the year and are stretched over a scale of several tens of meters; these are thus easier to discern.

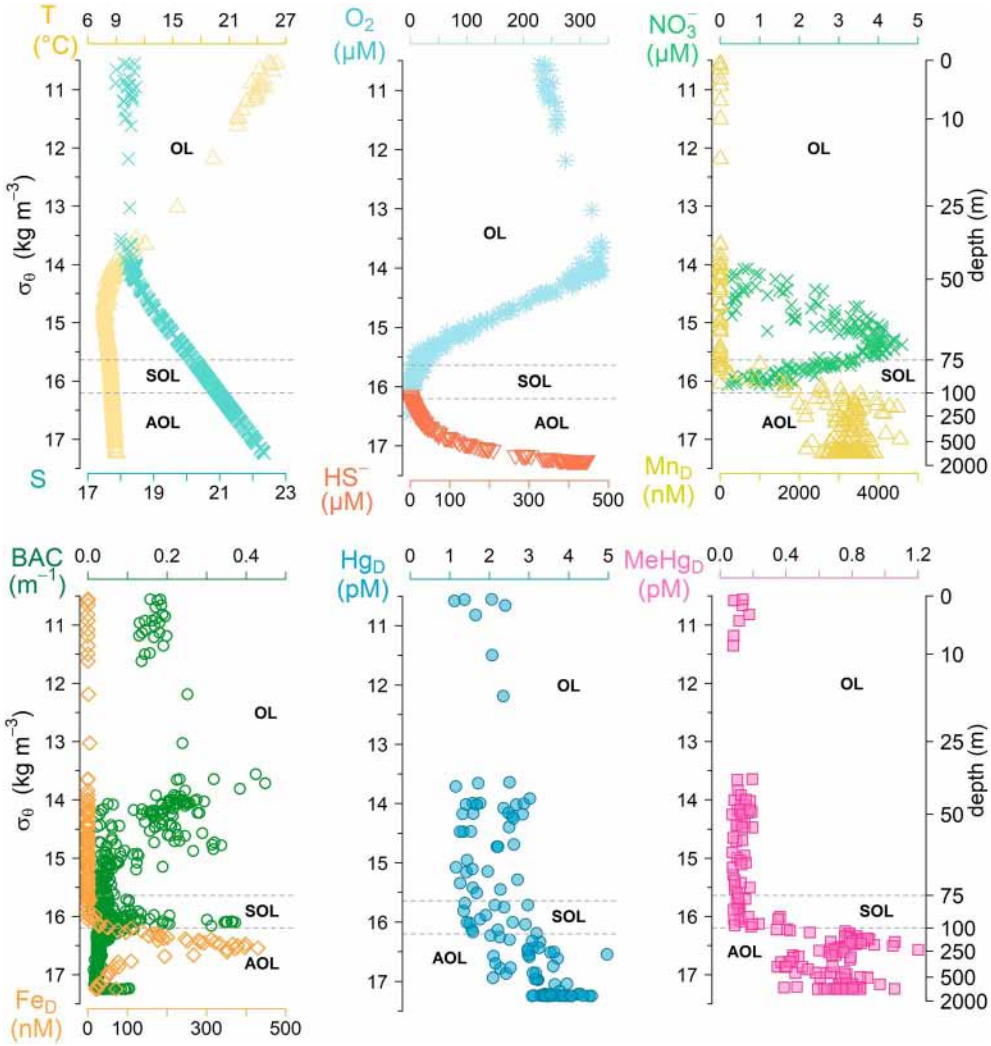

Figure 2. Biogeochemical features of the water column (stations 1–10) illustrated by the observed vertical profiles of temperature (*T*), salinity (*S*), oxygen (O_2), hydrogen sulfide (HS^-) beam attenuation coefficient (as a proxy of suspended particulate matter), dissolved manganese (Mn_D), dissolved iron (Fe_D), nitrate (NO_3^-), dissolved Hg (Hg_D), and MeHg ($MeHg_D$). The potential density anomaly ($\sigma_\theta = \sigma(S, \theta, 0) - 1{,}000$, kg m^{-3}) is used as a vertical axis to study homogeneous water masses (see main text). The boundaries of the redox layers computed from the cruise data set are shown in each panel (OL = oxic layer; SOL = suboxic layer; AOL = anoxic layer).

The sequence of redox reactions driving NOM remineralization in the water column is mirrored by the concentration profiles of the electron acceptors (Figure 2). The upper part of the oxic layer (OL) is euphotic (~50 m depth) with high O_2 concentrations (~300 μM), while below, in the aphotic waters, O_2 is gradually consumed by nitrifying bacteria (oxycline), as revealed by increasing NO_3^- concentrations (Oguz et al., 2000). The suboxic layer (SOL) at a depth of approximately 100 m is where concentrations of both oxygen and sulfides are extremely low ($O_2 < 20$ μM, $HS^- < 1$ μM). The upper boundary of the anoxic layer (AOL) occurs at a depth of approximately 140 m, and sulfide levels increase within the AOL down to the seabed (2,200 m depth) (Murray et al., 2007). The boundaries between the redox layers occur at variable depths, depending on the bathymetry and hydrographical region, but they are distributed along isopycnals (Konovalov et al., 1997). Therefore, the use of density (σ, see section 2.2) as a vertical coordinate has been a standard approach in studies dealing with the Black Sea since the early 1990s (Konovalov et al., 2004).

This paper aims to understand Hg speciation along a redox gradient by focusing on the pathways of MeHg production and transport. We integrated novel marine Hg and MeHg observations from the 2013 GEOTRACES MEDBlack cruise with a fate and transport 1-D model for Hg species (Melaku Canu et al., 2015) adapted from the

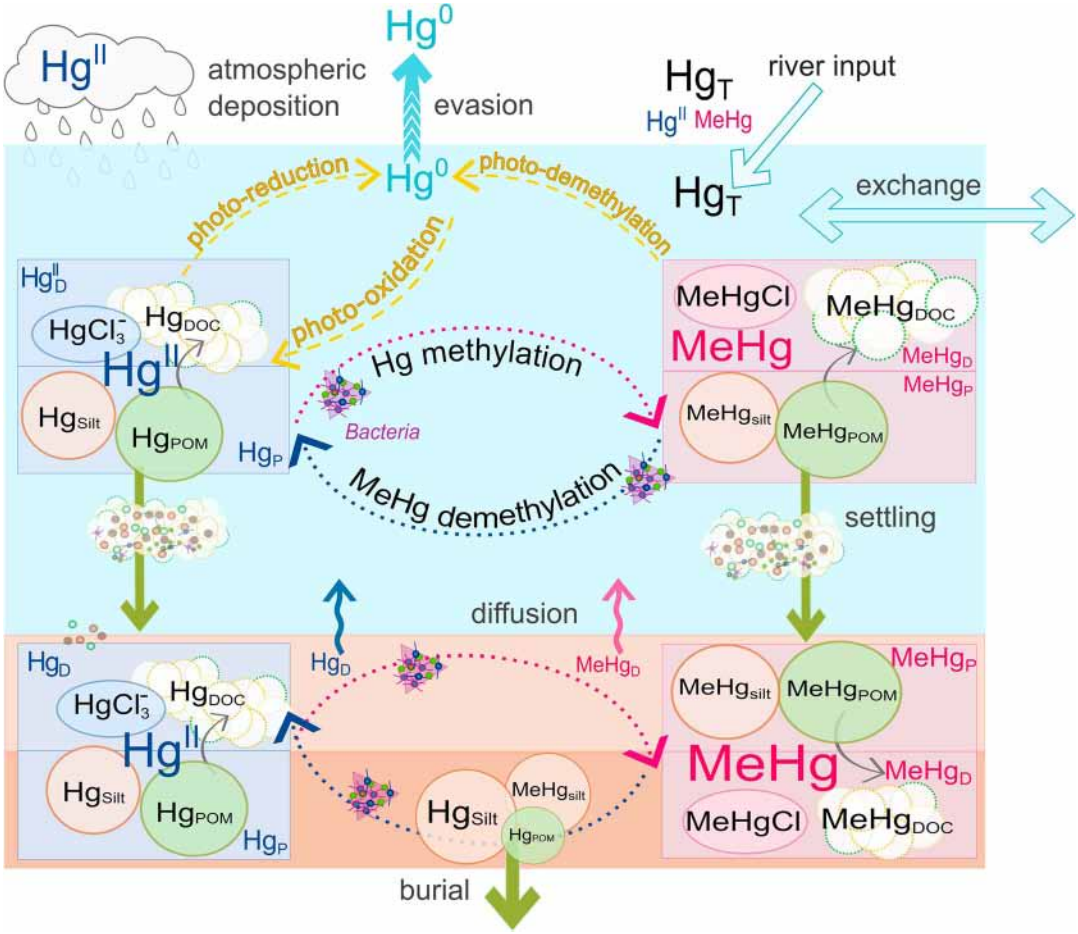

Figure 3. Overview of Hg species and processes simulated in the WASP7 MERC model. Hg_T is total Hg (Hg^{II} + Hg^0 + MeHg). Hg_P and $MeHg_P$ are Hg^{II} and MeHg bound to particulate organic matter or silt, while Hg_D and $MeHg_D$ are dissolved forms of Hg^{II} and MeHg (ionic and dissolved organic carbon complexed). Transformations (dashed arrows) include photochemical (Hg^{II} photoreduction, Hg^0 photooxidation, and MeHg photodemethylation) and biological (methylation and demethylation) processes. Transport processes include atmospheric deposition and evasion, input from rivers, exchange driven by advection and diffusion, and transport of Hg_P and $MeHg_P$ (settling, deposition, and burial).

WASP7 Hg model /MERC7 sub-model (Wool et al., 2001) and already succefully applied in shallow waters (Canu & Rosati 2017; Melaku Canu et al., 2015). One-dimensional (1-D) modeling has widely been used to investigate the biogeochemical and ecological features of the basin (Grégoire & Soetaert, 2010; Konovalov et al., 2004; Lamborg et al., 2008; Oguz et al., 2000; Yakushev et al., 2007). The implementation of the WASP7 model requires a careful compilation of Hg fluxes within the basin, which includes exchanges with the Marmara Sea, rivers and the atmosphere, and water-sediment exchanges and burial (Figure 3). We computed the budget of Hg species and used the model to assess the occurrence of Hg methylation and MeHg demethylation along the extended redox gradient of the Black Sea water column. Furthermore, we ran additional simulations to test the hypothesis that Hg methylation occurs exclusively in suboxic waters and is inhibited in the anoxic waters, as proposed by Lamborg et al. (2008). The authors detected a MeHg maximum in the SOL and very low levels in the AOL during a previous assessment of Hg species dynamics in the Black Sea. The model was also used to estimate the amount of anthropogenic Hg in the Black Sea water.

2. Materials and Methods

2.1. Sampling and Laboratory Analysis

Samples were collected during the second leg of the 2013 GEOTRACES MEDBlack (GA04-leg2) cruise in the Black Sea. The research vessel Pelagia occupied 12 full-depth stations in the Black Sea along an east-west transect between 13 and 25 July 2013. High-resolution vertical profiles, including one ultrahigh-resolution

profile (5 m steps), were sampled using a titanium ultraclean conductivity-temperature-depth frame (De Baar et al., 2008) equipped with 24 × 24 L polyvinylidene fluoride samplers. Samples were filtered (0.2 μm, Sartobran 300), drawn directly into individual precleaned 250 mL perfluoroalkoxy Teflon bottles (Savillex Purillex™), and acidified to 0.4% (v:v) with double-distilled HCl. We also sampled one station (40.8333°N, 27.56667°E, Figure 1a) in the Marmara Sea (Mediterranean Sea) during the first leg of the 2013 GEOTRACES MEDBlack cruise (GA04-leg1) to obtain Hg_D and $MeHg_D$ data that we used to parametrize the inflow and outflow to the Black Sea.

Total Hg_D was measured in a 35 mL aliquot following the USEPA 1631 method, which was modified for ultralow-level seawater measurements (Heimbürger et al., 2015). Potassium bromide (Sigma-Aldrich, USA) and potassium bromate (Sigma-Aldrich, USA) were heated for 4 h at 250°C to remove Hg traces before preparing a BrCl solution with freshly double-distilled HCl. We used a custom-made semi-automatic single gold trap setup coupled to a cold vapor atomic fluorescence spectrometer (Brooks Rand Model III, USA), modified with a mirrored quartz cuvette (Hellma Optics, Germany).

We measured dissolved methylmercury ($MeHg_D$) as the sum of monomethylmercury and dimethylmercury (MMHg + DMHg). $MeHg_D$ was analyzed via isotope dilution (ID) using a high-sensitivity coupled gas chromatograph-sector field ICP-MS (GC-SF-ICP-MS) (Heimbürger et al., 2015). Briefly, enriched spikes of ^{199}iHg and ^{201}MeHg (ISC Science, Spain) were added to a 115 mL aliquot of the seawater samples. After 24 h equilibration, the pH was adjusted to 3.9 with NH_3 (ULTREX® II Ultrapure Reagent, J.T. Baker, USA) and a buffer solution of acetic acid (glacial, ULTREX® II Ultrapure Reagent, J.T. Baker, USA)/sodium acetate (J.T. Baker, USA). Sodium tetra propyl borate (1 mL, 1%, v:v; Merseburger Spezialchemikalien, Germany) was then added to 200 μL hexane (Sigma-Aldrich, USA). The glass bottles were hermetically sealed with Teflon-lined caps and vigorously shaken for 15 min. The organic phase was recovered, and 2 μL was injected into the GC (Thermo Trace Ultra) coupled to a SF-ICP-MS (Thermo Element XR). Initial results indicated undetectable amounts of MeHg in the anoxic waters. However, we also did not recover the added isotopic spikes, indicating that our method was not appropriate for anoxic samples. Another acidified aliquot was oxygenated for 15 min after the spike addition and equilibration but prior to the derivatization step. This led to full spike recovery and significant amounts of MeHg detected in all samples. The detection limit was 0.025 and 0.001 pM for Hg_D and $MeHg_D$, respectively.

We took GEOTRACES intercalibration samples on 15 July 2013 in the western gyre (31.402°E; 42.521°N), in the oxic waters near the chlorophyll maximum (45 m depth) and sent these out to 25 participating laboratories. Our results compare well to consensus values: $Hg_T = 0.92 \pm 0.36$ pM, $n = 17$, $MeHg_T = 0.57 \pm 0.36$ pM, $n = 9$. We measured the GEOTRACES intercalibration sample three times for Hg_T and obtained 0.98, 0.95, and 0.96 pM, on 10 September 2013, 15 December 2013, and 30 October 2014, respectively. We determined 0.091 and 0.063 pM of MeHg on 10 September 2013 and 15 December 2013, respectively.

2.2. Vertical Discretization of the Data Set

We analyzed the vertical distribution of physical properties, nutrients, and metals at 10 deep stations of the 2013 GEOTRACES MEDBlack cruise (Gerringa et al., 2016; Margolin et al., 2016), excluding station 12, which is in the Bosporus Strait, and station 11, which is shallow and influenced by the Mediterranean inflow. Many authors (e.g., Konovalov & Murray, 2001) have already observed that, due to the distribution of water masses along isopycnals, the profiles of several variables show a strong similarity when plotted against density but differ when depth is used (Figures 2, S1, and S2). As depth increases, the adiabatic compression on water molecules causes a temperature increase that leads to an apparent decrease in density ($\rho(S, T, p)$, kg m^{-3}). To compare the density of two parcels of water from different depths, is recommended the use of potential density anomaly ($\sigma_\theta = \sigma(S, \theta, 0) - 1000$, kg m^{-3}), which is computed from potential temperature (θ) defined as "the temperature that a water parcel would have if moved adiabatically to another pressure" (Talley et al., 2011). To exclude possible outliers, we first analyzed Hg_D and $MeHg_D$ profiles (up to 2,160 m depth; $\sigma_\theta = 17.25$) by discretizing the water column using fine resolution (Table S1). This partitioning is appropriate to handle outliers and define the average concentration profile of metals and nutrients, but it is too detailed for our modeling purposes. A vertical discretization model (Table 1 and Figure 1b) was used in order to decompose the water column into its redox layers (OL, SOL, and AOL), further dividing some layers to properly represent the water balance of the system and simulate the evolution of the target variables (Hg, MeHg, and POM). Thus, the OL and AOL were divided into four sublayers each (namely, from O1 to O4, and from A1 to A4), and the sediments were divided into two sublayers (SED1 and SED2).

Table 1
Physicochemical Properties of Water and Sediment Layers and Sublayers

Redox layer	Model layer	Depth (m)	σ_θ (kg m^{-3})	Volume (m^3)	E_z[a] (m^2 s^{-1})	O_2 (μM)	HS^-(μM)	Hg (pM)	MeHg (pM)	MeHg/Hg (%)
OL (oxic layer)	O1	0–20	10.50–12.05	5.9×10^{12}	1.1×10^{-5}	246	0	1.86	0.12	8.5
	O2	20–40	12.05–14.25	5.9×10^{12}	1.1×10^{-5}	315	0	2.13	0.14	6.4
	O3	40–55	14.25–15.18	4.5×10^{12}	9.5×10^{-6}	165	0	1.77	0.12	9.9
	O4	55–75	15.18–15.64	5.9×10^{12}	9.5×10^{-6}	31.3	0	1.90	0.11	5.5
SOL (suboxic layer)	S	75–100	15.64–16.2	7.4×10^{12}	9.5×10^{-6}	3.5	0.1	2.06	0.16	10.9
AOL (anoxic layer)	A1	100–280	16.2–16.6	5.3×10^{13}	1.0×10^{-5}	0	15	3.16	0.80	28.6
	A2	280–460	16.6–17.04	5.3×10^{13}	1.0×10^{-5}	0	97	2.81	0.55	21.8
	A3	460–1460	17.04–17.24	2.9×10^{14}	5.5×10^{-6}	0	317	3.71	0.75	21.0
	A4	1460–1810	17.24–17.25	1.0×10^{14}	8.7×10^{-6}	0	421	3.71	0.74	20.6
Sediment	SED1			8.8×10^{9}	—					
	SED2			2.0×10^{10}	—					

Note. For each model layer are given: the depth and density range, the volume, the vertical eddy diffusivity (E_z) and the observed average concentrations of oxygen, sulfide, dissolved Hg and MeHg, and the MeHg%.
[a]E_z: vertical eddy diffusivity from Konovalov et al. (2004).

2.3. Model Structure

The WASP7 Hg model/MERC7 submodel (Wool et al., 2001) is a dynamic process-based model designed to simulate the Hg cycle within a system of well-mixed discrete spatial units (layers) of water and sediment as well as the exchanges of the system with its boundaries. This model has been already adapted and successfully applied to a shallow environment in a 2D configuration (Canu & Rosati, 2017; Melaku Canu et al., 2015), and is here used in a 1D configuration to explore Hg dynamics along an extended redox gradient.

Figure 3 shows the conceptual model of the processes that affect the evolution of the state variables (Table S2). Modeled Hg species (Table S3) include dissolved and particulate compounds of oxidized Hg (Hg^{II}), elemental mercury (Hg^0), and methylmercury (MeHg), whereas dimethylmercury (DMHg) is not explicitly considered. Dissolved species include Hg^0, dissolved organic carbon (DOC)-complexed species of Hg^{II} and MeHg (i.e., Hg_{DOC} and $MeHg_{DOC}$), and their ionic species ($HgCl_3^-$, $HgCl_4^{2-}$, and MeHgCl) in marine environments (Morel et al., 1998). Particulate species involve only Hg^{II} and MMHg, which in the model can be adsorbed to POM (Hg_{POM} and $MMHg_{POM}$) or silt (Hg_{silt} and $MMHg_{silt}$); silt represents inorganic particles, and POM is used to represent both organic particles and Fe/Mn oxides that are subjected to precipitation and dissolution. POM is modeled as a state variable that can be produced and decomposed according to the formulas given in Table S4, while DOC is modeled as constant in time, with different concentrations in each box according to Ducklow et al. (2007) and Margolin et al. (2016).

Hereafter, we refer to total Hg (Hg_T) and total MeHg ($MeHg_T$) as the sum of all Hg and MeHg species in the dissolved and particulate phases. We refer to dissolved Hg (Hg_D) to indicate the sum of all dissolved species (Hg^0, Hg_{DOC}, $MeHg_{DOC}$, $HgCl_3^-$, $HgCl_4^{2-}$, and MeHgCl), while dissolved Hg^{II} and MeHg (Hg_D^{II} and $MeHg_D$) will be used to indicate, respectively, the sum of $Hg_{DOC} - HgCl_n$ and $MeHg_{DOC} - MeHgCl$. We will refer to particulate Hg (Hg_P) as the sum of inorganic Hg particle-bounded species (Hg_{POM} and Hg_{silt}) and refer to particulate MeHg ($MeHg_P$) as the sum of $MeHg_{POM}$ and $MeHg_{silt}$.

The main transport (i.e., diffusion, advection, volatilization, deposition, settling, and burial) and transformation (i.e., biotic methylation and demethylation, photoreduction, photooxidation, and photodemethylation) processes related to the Hg cycle are considered in the model (Tables S3–S6). Resuspension does not occur in the deep water of the Black Sea due to low turbulence (Stanev & Kandilarov, 2012), and thus, it is not included in our model (Table S7). Transport processes (Tables S5) are described through advective water fluxes, diffusion coefficients, and transport mediated by particles. Hg transformation processes (Tables S6) are modeled using first-order kinetics, through a reaction constant (k_r) modulated based on environmental forcing such as temperature and light intensity.

2.4. Model Physical and Biological Setting

We represent the Black Sea as a 1-D vertical system with nine layers of water and two layers of sediment (Table 1). Since we aimed to simulate the dynamics in the offshore basin of the Black Sea, the shelf area

was excluded from analysis (~30% of surface area) (Panin & Jipa, 2002), constraining the model domain to represent 70% of the volume of the upper water and 100% of the deep water, overall accounting for 99% of the total volume. The steady state balance of water masses (Text S1 and Figure 1b) was arranged according to Özsoy and Ünlüata (1997), and turbulent vertical diffusion (E_z; Table 1) was set according to Konovalov et al. (2004). Monthly averaged data for solar irradiation, day length, and sea surface temperature for the Black Sea in the year 2013 (Gencarelli et al., 2015; Grell et al., 2005) were used as forcing for photoreactions, biological reactions, and volatilization. To satisfy the sediment balance of the Black Sea (Text S2, Figure S3, and Tables S4 and S8), we considered silt and POM exchanges with the Marmara Sea (Mediterranean Sea) (Çoban-Yıldız et al., 2000, 2006), loadings from rivers and the Azov Sea (Agapov et al., 2012; Berlinsky et al., 2006; Chasovnikov et al., 2012; Jaoshvili, 2002; Ovsienko et al., 2012; Panin & Jipa, 2002; Tescari et al., 2006) and internal POM production and degradation, including both primary production (Agirbas et al., 2014) and chemosynthesis (Nyffeler et al., 2007; Yılmaz et al., 2006). POM degradation rates were calibrated in agreement with the carbon budget (Deuser, 1971; Grégoire & Soetaert, 2010; Margolin et al., 2016), and 80% of suspended particles in the model is POM, in agreement with Stanev and Kandilarov (2012). Total suspended particles were calibrated to match concentrations (Figure S4) estimated from the beam attenuation coefficients (Karageorgis et al., 2008, 2009) measured during the cruise, which are in good agreement with those given in Stanev and Kandilarov (2012). For the sediment compartment, two layers were modeled: a 3 cm deep fluffy layer with porosity of ~0.96 (Yücel et al., 2012) on top of a 7 cm deep layer of more consolidated sediment.

2.5. Mercury Species Data and Time Dynamic Model Implementation

To simulate the historical evolution of Hg dynamics in the Black Sea in our 1-D model, we took into account the inputs and outputs of the system, transport mediated by water and sediment, and transformation processes (Tables S2–S8). We chose to reconstruct past inputs into the Black Sea because the residence time of the deep water has been estimated to be between 330 and 1,500 years (Murray et al., 2007), and thus, present-day concentrations in the deep water must reflect processes that have occurred over long periods. As anthropogenic Hg emissions increased dramatically with the onset of the industrial revolution (Amos et al., 2015), we estimated the temporal evolution of Hg inputs beginning in 1850, assuming that prior inputs are negligible for the Hg dynamics in the Black Sea. We gathered information about Hg species loads, boundary concentrations, and fluxes for the year 2013 (Tables S7–S9) and rescaled riverine and atmospheric Hg input according to historical anthropogenic enrichment factors estimated for global emissions and the deposition of Hg (Amos et al., 2015; Horowitz et al., 2014). The model was initialized at a pristine level, with 0.14 pM of Hg^{II}, 0.02 pM of Hg^0 in surface waters, and 0.3 pM of Hg^{II} in the waters below 100 m depth (Zhang Jaeglé, & Thompson, 2014); water MeHg was assumed to be 5% of Hg_T. Hg sediment concentration was set to 235 pmol g^{-1} (47 ng g^{-1}) based on the background Hg concentrations of sediment cores taken during the 2013 GEOTRACES MEDBlack cruise. The background Hg levels are 3.4 times lower than present-day surface level and do not show any influence of preindustrial Hg enrichments, supporting the idea that anthropogenic Hg inputs to the Black Sea prior 1850 are negligible. The simulation was projected to the year 2050, assuming that future Hg input will remain constant at 2013 levels.

Atmospheric concentrations of Hg^{II} and Hg^0 and fluxes of Hg^{II} deposition (Table S7) over the Black Sea (year 2013) were computed with the Weather Research and Forecasting Model with Chemistry-Hg atmospheric model (Gencarelli et al., 2014, 2015, 2017). The atmospheric model was forced with the chemical initial and boundary conditions for Hg species taken from the ECHMERIT model (De Simone et al., 2014, 2016; Jung et al., 2009), and the model domain was adapted to include the entire Black Sea surface area; further information is given in Text S3 (Arctic Monitoring and Assessment Programme/United Nations Environmental Programme, 2013; Emmons et al., 2010; Gårdfeldt et al., 2003; Grell et al., 2005; Lin et al., 2006; Neu & Prather, 2012; Salzmann & Lawrence, 2006; Sandu & Sander, 2006; Wanninkhof, 1992; Wesely, 1989). Marine boundary conditions for Hg and MeHg were characterized based on measured concentrations in the Marmara Sea (Table S7) and hydrodynamics (Figure 1b and Text S1); Hg^0 concentrations were assumed to be 10% of Hg_T (Fantozzi et al., 2013; Gårdfeldt et al., 2003; Kotnik et al., 2015; Soerensen et al., 2013). Photoreaction rates (Table S9) are internally adjusted for the light conditions following Soerensen, Schartup, et al. (2016). These processes are relatively well constrained; others are much less: (1) the partitioning of Hg, which is parameterized through the partition coefficient (k_D, l/kg) for which a wide range is reported in the literature (Han, Lehman, et al., 2007; Han, Obraztsova, et al., 2007; Hollweg et al., 2010; Lamborg et al., 2016; Liu

et al., 2015; Muresan et al., 2007; Schartup et al., 2014, Schartup, Balcom, et al., 2015); (2) the Hg river inputs (Tables S7 and S8) (Amos et al., 2014; Soerensen, Schartup, et al., 2016; Woitke et al., 2003; Zhang et al., 2015), with the fraction of river MeHg being generally low (~5% of Hg_T) (Balogh et al., 2003; Mason et al., 2012; Paller et al., 2004; Sharif et al., 2014; Soerensen, Jacob, et al., 2016, Soerensen, Schartup, et al., 2016); and (3) Hg methylation and MeHg demethylation (Hsu-Kim et al., 2013; Semeniuk & Dastoor, 2017).

A separated model setup was implemented to simulate the preanthropogenic cycle of Hg in the Black Sea by running two additional simulations forced only with natural Hg inputs (upper and lower estimates). Natural river inputs were assumed to be 0.4%–16% of present-day inputs (corresponding to Hg_P = 0.01–0.1 nmol g^{-1} that is in the lower range of the assessment by Amos et al. (2014)) and natural Hg atmospheric deposition to be 13–20% of present-day deposition (Zhang, Jaeglé, Thompson, & Streets, 2014). Results of these simulations were used to estimate the anthropogenic Hg in the Black Sea relative to the base simulation.

2.6. Model Calibration and Analysis of Uncertainties in Parameters and Model Output

Monte Carlo analysis (i.e., analysis of an ensemble of numerical simulations) can be useful to estimate uncertain model parameters while maintaining a reasonable fit to observations (Beck, 1987; Cossarini & Solidoro, 2008; Jørgensen, 1994; Pianosi et al., 2016; Soetaert & Herman, 2009). Here we constrained the most uncertain processes/parameters to observed concentration of Hg_D and $MeHg_D$ in the water column and Hg_T in sediment, by using a two steps procedure involving an ensemble of simulations. In the first step, we derived the most likely estimates of river loads and partition coefficient (k_D) against water Hg_D and sediment Hg_T observations. In the second step, the model was refined and calibrated to observational data of water $MeHg_D$ and Hg_D, by tuning the Hg methylation and demethylation rates (k_m and k_{dm}). The agreement between modeled (mod_i) and observed (obs_i) concentrations in waters and sediment for the reference year (2013) was evaluated for each sensitivity simulation by computing the Pearson's correlation coefficients (r) and the root-mean-square errors (RMSE, equation (1)).

$$\mathrm{RMSE} = \sqrt{\frac{\sum_{i=1}^{n}(\mathrm{obs_i} - \mathrm{mod_i})^2}{n}} \tag{1}$$

As a first step, we run an ensemble of simulations excluding biotic production and degradation of MeHg within the system. Each simulation was performed by using the same values for all parameters but for k_D and the time-variable river load ($L_{r(t)}$), which were varied within a large interval, namely, k_D 5×10^5–6.2×10^5 l/kg, and $L_{r(2013)}$ 15–40 kmol/yr ($L_{r(t)}$ were derived from $L_{r(2003)}$ by backward scaling, according to Horowitz et al. (2014), to simulate the historical evolution). Then we compared each simulation against observations and rejected all the simulations that have $r < 0.9$, RMSE for water $Hg_D > 0.8$ pM, and RMSE for sediment $Hg_T > 300$ pmol g^{-1}. The subset of remaining simulations (the ones with a good fit to observations) was retained, and the corresponding parameters values were used to estimate the distribution (given as mean ± standard error (SE)) of: $L_{r(2013)} = 25 \pm 2.5$ kmol yr^{-1} and $k_D = 5.6 \times 10^5 \pm 9.3 \times 10^4$ l/kg. The simulation from this subset that reproduces the average water Hg_D and sediment Hg_T concentrations is hereafter referred to as reference simulation. The other simulations with a good fit to observations were used to compute the SE of modeled concentrations, which is related to the uncertainties in k_D and L $L_{r(2013)}$.

In the second step, we performed a second ensemble of simulations, starting from the reference simulation obtained in step 1 and adding in Hg methylation and MeHg demethylation rates (k_m and k_{dm}) in the different water layers. In this case we identified the variability interval by selecting k_m and k_{dm} values for different redox conditions within literature ranges (Table S10) (Hollweg et al., 2009; Lehnherr et al., 2011; Monperrus, Tessier, Amouroux, et al., 2007; Rodríguez Martín-Doimeadios et al., 2004; Whalin et al., 2007) and by varying the selected rates by ±50% (Table 2). To gain insights into the significance of these processes in the redox layers of the Black Sea (OL, SOL and AOL), we set up three different scenarios (Table 2) based on the following hypotheses:

1. ubiquitous Hg methylation and MeHg demethylation;
2. Hg methylation is limited to the SOL, ubiquitous MeHg demethylation;
3. Hg methylation and MeHg demethylation are both limited to the SOL.

As before, we rejected the simulations that did not have a sufficient fit with the data and used the subset of retained simulation (those having r for water $MeHg_D$ and $Hg_D > 0.9$ as well as RMSE for water

Table 2
Parameterization of Hg Methylation (k_m) and MeHg Demethylation (k_{dm}) in the Simulations: a) Ubiquitous k_m and k_{dm}; b) k_m Limited to the SOL and Ubiquitous k_{dm}; c) k_m and k_{dm} Limited to the SOL

	a) Ubiquitous Hg methylation and MeHg demethylation		b) Hg methylation in the SOL, ubiquitous MeHg demethylation		c) Hg methylation and MeHg demethylation limited to the SOL	
Layer	k_m (d^{-1})	k_{dm} (d^{-1})	k_m (d^{-1})	k_{dm} (d^{-1})	k_m (d^{-1})	k_{dm} (d^{-1})
OL	4×10^{-3} [±50%]	1.0×10^{-1} [±50%]	0	1.7×10^{-2} [±50%]	0	0
SOL	1.6×10^{-2} [±50%]	2.1×10^{-1} [±50%]	1.6×10^{-2} [±50%]	2.1×10^{-1} [±50%]	1.6×10^{-2} [±50%]	2.1×10^{-1} [±50%]
AOL	3.3×10^{-3} [±50%]	1.5×10^{-2} [±50%]	0	1.5×10^{-2} [±50%]	0	0

Note. See Table S10 for literature ranges of k_m and k_{dm} under different redox conditions. OL = oxic layer; SOL = suboxic layer; AOL =anoxic layer.

$MeHg_D < 0.2$ pM and RMSE for water $Hg_D < 0.35$ pM). Obviously, to take into consideration the uncertainties in k_m and k_{dm} values produces some variability in model output. However, from the analysis of the second ensemble of simulations it turned out that such variability is significantly smaller than the one related to the parameters variation in the first calibration step (not shown) and that the tuning of k_m and k_{dm} induced minor variations in the fit against water Hg_D and sediment Hg_T. Finally, we selected the model ensemble giving the best fit to data and use that to define the fluxes and related uncertainties in a budget of Hg species in the Black Sea.

3. Results and Discussion

3.1. Observations

Hg_D and $MeHg_D$ vertical profiles show similar behavior across the 10 deep stations sampled in the Black Sea (Figures 2, S1, and S2), suggesting that all stations can be described in terms of a similar dynamic along the vertical dimension. Thus, a 1-D representation of the system seems suitable to capture the most important dynamics of Hg in the Black Sea. Concentrations in the OL and SOL are lowest (Hg_D = 1.9 ± 0.6 pM; $MeHg_D$ = 0.13 ± 0.05 pM) and do not differ from each other (Wilcoxon signed-rank test; p value >0.05), while concentrations in the AOL (Hg_D = 3.4 ± 0.6 pM; $MeHg_D$ = 0.71 ± 0.17 pM) are significantly higher (Wilcoxon signed-rank test; p value <0.05). Both Hg_D and $MeHg_D$ concentrations exhibit two maxima in the AOL: the first one is just below the SOL-AOL interface and the second one in the deep part of the AOL. While the Hg_D and $MeHg_D$ profiles mimic each other, the relative MeHg increase from SOL to AOL (+340%) is more important than the Hg_D increase (+62%), suggesting that production of MeHg occurs in the AOL. Figure 2 shows the vertical distribution of Hg_D, $MeHg_D$, and other biogeochemical variables against σ_θ, while Figure 4 shows the distribution of $MeHg_D$ against depth along the cruise transect. The average concentrations of Hg_D, $MeHg_D$, O_2, and HS^- are given in Table 1, and the complete data set of Hg and MeHg observations is available in Table S11.

The first maxima of Hg_D and $MeHg_D$ (Figures 2 and 5) occur at 100–200 m depth in the upper part of the AOL (σ_θ 16.3–16.5). We found that the Hg_D and $MeHg_D$ maxima are broadly coincident with the Fe_D and/or Mn_D (Figure 5) in the Black Sea water column, as previously observed for Hg_D and Mn_D/Fe_D (Lamborg et al., 2008) as well as for Hg_T and Fe_D/Mn_D (Cossa & Coquery, 2005). The association between Hg species and Mn/Fe redox cycles is usually explained by the "shuttle theory" that postulates a transportation process based on Mn/Fe oxides (Neretin et al., 2003). According to this theory, Hg is scavenged from surface layers by POM and Mn/Fe oxides and settles toward the bottom of the SOL, where oxide reduction drives NOM remineralization, causing Hg_D release. Reduced Mn/Fe diffuses upward and is oxidized at the top of the SOL; likewise, Hg_D released in the AOL diffuses upward and is scavenged by oxides. Therefore, Hg species are trapped in this cycle between the SOL and AOL. This process has been invoked to explain the distribution of phosphates in the Black Sea (Dellwig et al., 2010; Pakhomova & Yakushev, 2013; Shaffer, 1986) and the distribution of Hg species in stratified water bodies with anoxic bottom water (Cossa & Coquery, 2005; Han, Lehman, et al., 2007; Mason et al., 1993). The partition coefficients (K_D) of Hg to oxides have been shown to be higher than the range generally observed in sediments; Lamborg et al. (2016) estimated a $K_{D\text{-}Mn} = 10^{8.3}$, and $K_{D\text{-}Fe} = 10^{7.6}$ for Hg_T in the ocean. In the Black Sea, Mn is much more abundant than Fe (Figures 2 and 5) and likely

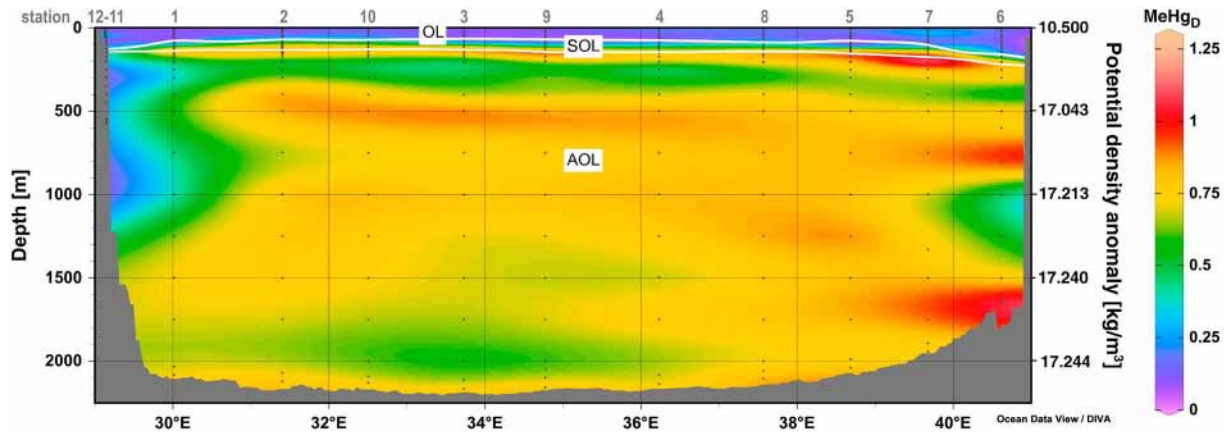

Figure 4. Distribution of $MeHg_D$ (pM) along 2013 GEOTRACES MEDBlack cruise transect. The numbers of the sampling stations (Figure 1) are given on the top of the figure. Black dots indicates sampling points. The contours of the oxic layer (OL), suboxic layer (SOL), and anoxic layer (AOL) are indicated by white lines.

plays a major role. As shown in Figure 5, concentrations of dissolved Mn (Mn_D) in the Black Sea rise in the SOL, peak below the SOL-AOL interface (σ_θ ~ 16.3) and remain elevated and constant until the seabed. Fe oxide reduction follows Mn oxide reduction in the sequence of electron acceptors used by bacteria for NOM remineralization (Froelich et al., 1979); indeed, the increase in dissolved Fe concentrations (Fe_D) is deeper than that of Mn_D, and Fe_D concentrations are maximal at σ_θ ~ 16.5. Below σ_θ ~ 16.5, Fe_D decreases due to precipitation as $FeS_{(s)}$ or $FeS_{2(s)}$; at this depth, there is a local minimum of Hg_D and $MeHg_D$ concentrations (Figures 2, S1 and S2), which might be due to their partial pyritization (coprecipitation) in the formation of FeS_2 (Huerta-Diaz & Morse, 1992; Morse & Luther, 1999). This process has also been proposed also for the

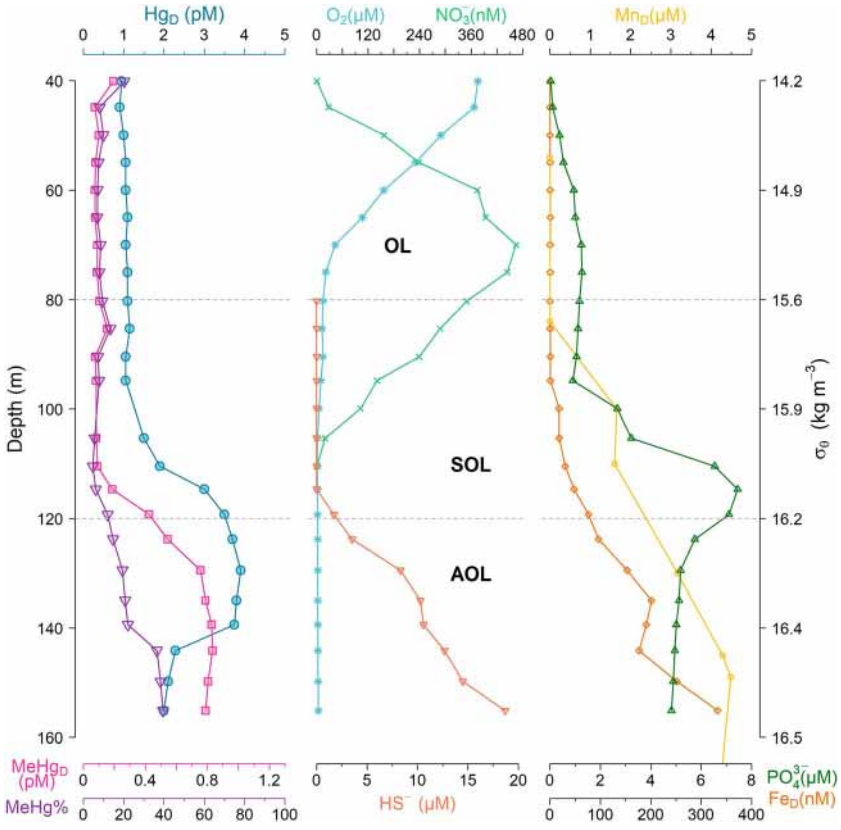

Figure 5. High-resolution profiles of dissolved Hg (Hg_D), and MeHg ($MeHg_D$), oxygen (O_2), hydrogen sulfide (HS^-), nitrates (NO_3^-), phosphates (PO_4^{3-}), manganese (Mn_D), and iron (Fe_D) at station 5 (Figure 1). OL = oxic layer; SOL = suboxic layer; AOL = anoxic layer.

cycling of Hg species in the Pettaquamscutt Estuary (Mason et al., 1993), while in Offatts Bayou (USA), it has been suggested to affect the water profile of Hg^{II} but not that of MeHg; this is likely because higher POM concentrations in the shallow bay outcompete FeS_2 for binding sites (Han, Lehman, et al., 2007).

Our high-resolution profiles (Figure 5), with 5 m sampling intervals covering the extended redox gradient from oxic waters (40 m depth) to anoxic waters (160 m depth) at station 5, allowed us to further resolve Hg distributions. The high-resolution Hg_D maximum (3.9 pM at 130 m depth) is shallower at the interface of the SOL and AOL, just below the PO_4^{3-} peak. The high-resolution $MeHg_D$ maximum (0.83 pM at 145 m depth) is 15 m deeper, coinciding with the Mn_D peak, well within the AOL. Mercury methylation may be highest here because of the continuous supply of Hg_D during the dissolution of Mn oxides. The MeHg/Hg percentage increases further with depth in the AOL, reaching 39% at a 160 m depth. It is remarkable that the MeHg/Hg percentages are comparable to other open-ocean subsurface maxima in oxic waters (Bowman et al., 2015, 2016; Cossa et al., 2009, 2011; Ganachaud et al., 2017; Hammerschmidt & Bowman, 2012; Heimbürger et al., 2015; Kim et al., 2017; Munson et al., 2015; Sunderland et al., 2009; Wang et al., 2012).

In the deeper part of the AOL ($\sigma_\theta > 17.04$), Hg_D and $MeHg_D$ concentrations increase to a second maximum (Figures 2, S1 and S2), which might be due to the enhanced solubility of Hg species in the presence of sulfides and DOM (Han, Lehman, et al., 2007; Mason et al., 1993; Ravichandran et al., 1998, 1999; Skyllberg, 2008; Slowey, 2010; Sunderland et al., 2006; Waples et al., 2005) and to net in situ methylation, which is favored by DOM (Graham et al., 2012; Moreau et al., 2015; Schaefer & Morel, 2009; Schaefer et al., 2011). It has been shown that in sulfidic systems, some DOM components (thiols, humic acids, and cysteine) delay or inhibit $HgS_{(s)}$ precipitation and favor its dissolution, leading to the formation of nanoparticles smaller than 0.2 μm (Deonarine & Hsu-Kim, 2009; Gerbig et al., 2011; Slowey, 2010): these nanoparticles can be methylated (Jonsson et al., 2012; Kucharzyk et al., 2015; Zhang, Kucharzyk, et al., 2014; Zhang et al., 2012). These processes appear to be favored by low Hg/DOM ratios and may provide a mechanistic explanation for the second maximum of $MeHg_D$ that we observed in the AOL, where the ratio Hg/DOM is as low as ~0.2 nmol Hg/mg DOM. Recent research has also shown that MeHg adsorbed to reduced sulfur groups on minerals (FeS_m, $HgS_{(s)}$ and $CdS_{(s)}$) and organic (thiols) surfaces can be methylated to dimethylmercury (DMHg) (Jonsson et al., 2016). We measured DMHg at stations 2 and 5. The results (not shown) were near the detection limit, and we therefore conclude that the DMHg is only a minor fraction of the MeHg pool in the Black Sea, in agreement with Lamborg et al. (2008), who found DMHg to be less than 10% of MeHg. Therefore, we only considered the dominant MMHg species in the numerical model (labeled as MeHg).

While our observations of two deep maxima of Hg_D are consistent with previous findings for both filtered and unfiltered Hg in the Black Sea (Cossa & Coquery, 2005; Lamborg et al., 2008), the distribution of $MeHg_D$ differs from that observed in the western gyre by Lamborg et al. (2008), who detected only a shallow $MeHg_D$ maximum at $\sigma_\theta \sim 16.2$ and decreasing concentrations toward the seabed. We believe that this discrepancy is due to different analytical methodologies. We applied an ID method that can assess recovery of the analytes (section 2.1), while Lamborg et al. (2008) did not use ID. Their method might not have been efficient for the analysis of anoxic Black Sea waters. On the other hand, our observations are consistent with the distribution of MeHg along the stratified water column of the Gotland Sea (Baltic Sea) (Soerensen, Schartup, et al., 2016) and the seasonally anoxic waters of Offatts Bayou (USA) (Han, Lehman, et al., 2007), where concentrations are minimal above the halocline and maximal in anoxic water. Sulfide levels in these two systems are lower but comparable (150–200 μM) to those of the Black Sea (Han, Lehman, et al., 2007; Neretin et al., 2003).

3.2. Modeled Concentrations and Fluxes

The three ensembles of simulations referring to scenarios a, b, and c were all derived adding Hg methylation and MeHg demethylation in the same reference simulation, which was obtained from the first step of calibration against concentrations of Hg_D in water (Figure 6a) and Hg_T in the sediment (Figure 6b). The three scenarios a, b, and c represent different hypotheses for Hg methylation and MeHg demethylation occurrence along the redox gradient (Table 2), which were explored during the second step of calibration by varying k_m and k_{dm} values.

Results show that the ensemble of simulations (a), representing ubiquitous Hg methylation and MeHg demethylation (Figure 7a), reproduces best the $MeHg_D$ profiles observed during the cruise ($r = 0.98 \pm 0.01$; RMSE = 0.15 ± 0.07 pM). When Hg methylation is considered to be limited to the SOL (Figures 7b and 7c),

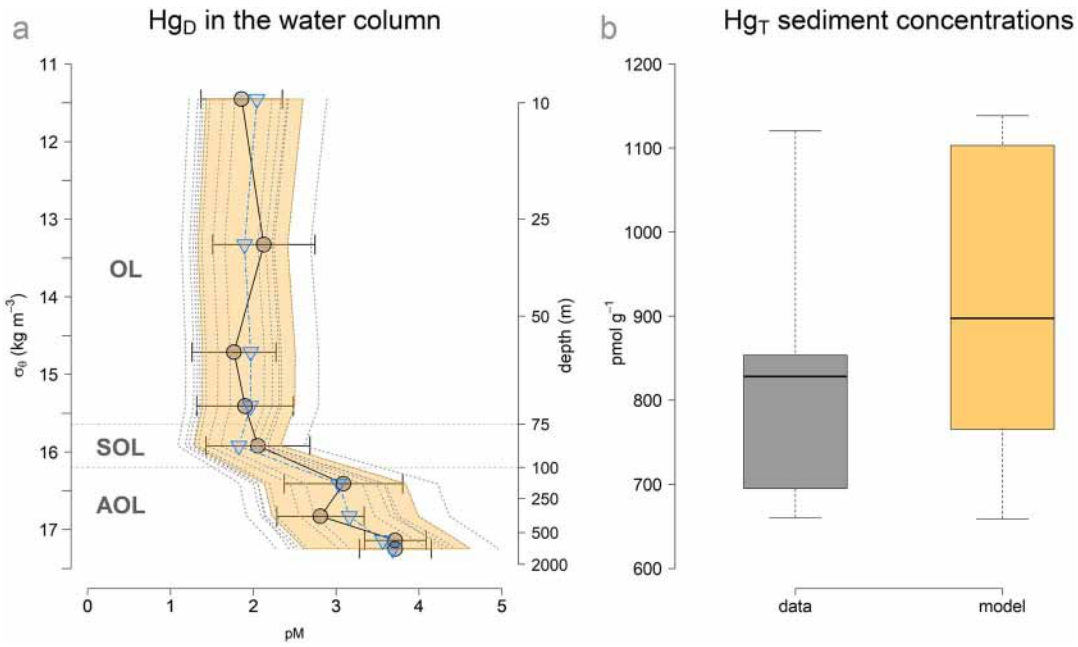

Figure 6. (a) Hg_D profiles in the water column observed during the cruise (black circles and bars: average and standard deviation of the 10 deep stations) and modeled (gray dashed lines: profiles from all simulations; yellow area: range estimated from the subset of simulations retained from the Monte Carlo ensemble (see section 2.6); blue triangles: reference simulation) by varying the river load and k_D. The potential density anomaly ($\sigma_\theta = \sigma(S, \theta, 0) - 1{,}000$, kg m^{-3}) is used as the vertical coordinate, and the corresponding depths are shown on the left *y* axes; (b) Hg_T concentrations in surface sediment (0–3 cm) observed during the cruise (gray box plot) and modeled (yellow box plot); each box plot indicates the median (thick bar), the interquartile range (box height), and the extremes of the distribution (whiskers). OL = oxic layer; SOL = suboxic layer; AOL = anoxic layer.

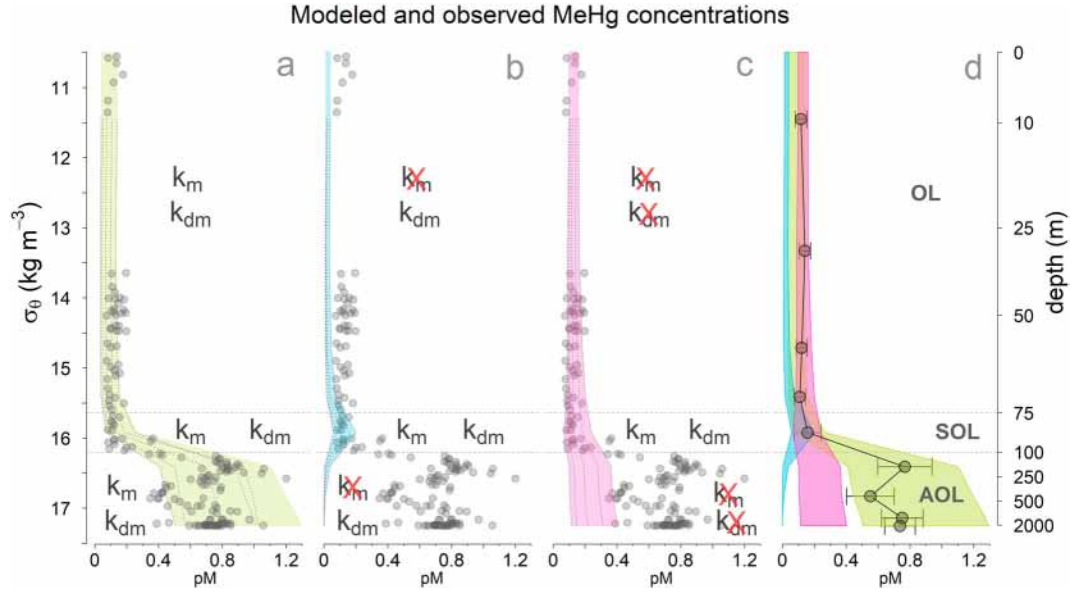

Figure 7. Distribution of $MeHg_D$ in the water column observed during the cruise (black dots, black circles and bars: data points, means, and standard deviation of the 10 deep stations) and range of modeled concentration (shaded areas) profiles from different simulations (gray dashed lines) run assuming: (a) ubiquitous k_m and k_{dm} (green area), (b) k_m limited to the suboxic layer (SOL) and ubiquitous k_{dm} (blue area), (c) k_m and k_{dm} limited to the suboxic layer (pink area), (d) all of the previous (Table 2). The potential density anomaly ($\sigma_\theta = \sigma(S, \theta, 0) - 1{,}000$, kg m^{-3}) is used as the vertical coordinate, and the corresponding depths are shown on the left *y* axes. OL = oxic layer; SOL = suboxic layer; AOL = anoxic layer.

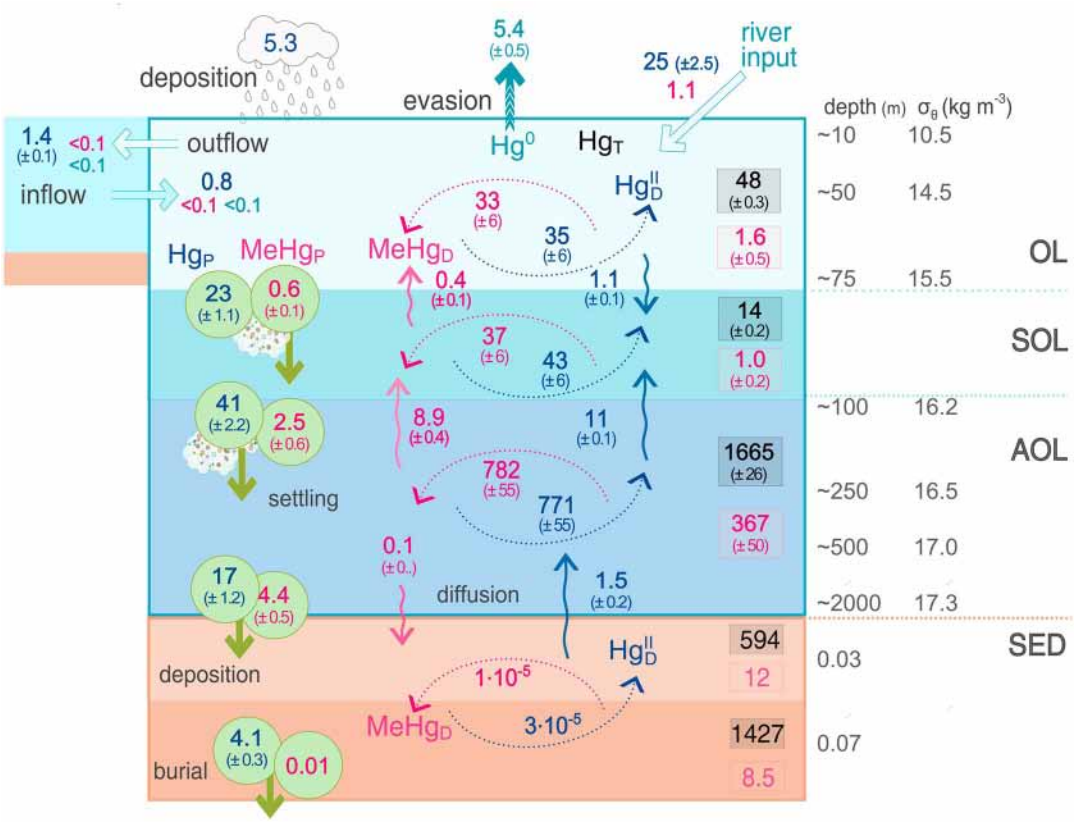

Figure 8. Budget for Hg species in the Black Sea. Modeled amount (kmol) and fluxes (kmol yr^{-1}) of Hg_T (black), Hg^{II} (blue) and $MeHg_T$ (pink) species in water and sediment layers, given as mean ± SE. Hg_T and $MeHg_T$ reservoirs (black and pink squares) are given on the right side. Hg^0 (dark cyan) is produced upon net photoreduction in oxic waters and mostly evade to the atmosphere; its pool is a minor fraction of the Hg_T pool and is thus omitted here. Settling, deposition and burial of Hg_P and $MeHg_P$ are represented by green circles and arrows. Fluffy arrows represent exchanges due to turbulent and molecular diffusion. Dashed arrows indicate methylation and demethylation. Thick arrows show exchanges at the model boundaries (atmospheric deposition and evasion, river load, and inflow-outflow to the Marmara Sea). On the right side depth and density scale are shown. OL = oxic layer; SOL = suboxic layer; AOL = anoxic layer.

the model cannot be tuned to reproduce the observed vertical MeHg distribution. The ensemble of simulations (b) have $r = -0.5 \pm 0.08$ and RMSE = 0.47 ± 0.01 pM, while simulations (c) have a better fit ($r = 0.93$ and RMSE = 0.34 ± 0.06 pM) but still significantly worse than (a). We conclude that observations and modeling falsify the hypotheses (b) and (c) and corroborate the hypothesis (a), that is, ubiquitous methylation and demethylation. Therefore, the setup (a) defines the most likely model given the available data.

We used the best model setup (scenario a), to compute concentrations and fluxes of Hg species (values are given as mean ± SE) in water and sediment of the Black Sea for the 2013 (Figure 8) and for the whole simulation period (1850–2050; Figure 9).

In its present state, Hg_T inputs to the water column (31 ± 2.5 kmol yr^{-1}) are estimated to exceed the outputs (28 ± 2.8 kmol yr^{-1}). The system is not at steady state, the $\Delta Hg_{T(2014-2013)}$ (difference of Hg pool between 2014 and 2013) is negative in the OL (−0.3 kmol yr^{-1}) and positive in the SOL and AOL (+0.04 and +0.52 kmol yr^{-1}). The most relevant input is riverine load (77%, 24.5 ± 2.5 kmol yr^{-1}), followed by atmospheric deposition (17%, 5.3 kmol yr^{-1}). Little Hg_T comes from sediment via pore water diffusion (4%, 1.4 ± 0.02 kmol yr^{-1}) from the Marmara Sea inflow (3%, ~0.9 kmol yr^{-1}) and from the Azov Sea (1%, ~0.4 kmol yr^{-1}, not shown). The main loss of Hg from the water (74%) is the settling and deposition of 20.9 ± 1.2 kmol yr^{-1} of Hg_P and $MeHg_P$. Evasion of Hg^0 (23%, 5.4 ± 0.5 kmol yr^{-1}) roughly compensates Hg^{II} deposition, and the outflow to the Marmara Sea accounts for 6% (1.4 ± 0.1 kmol yr^{-1}). The 26% of Hg that deposits to the sediment is buried below a 10 cm depth (4.1 ± 0.3 kmol yr^{-1}), while 8% moves back to the water through pore water diffusion; the remainder constitutes the sediment reservoir. The modeled reservoir of

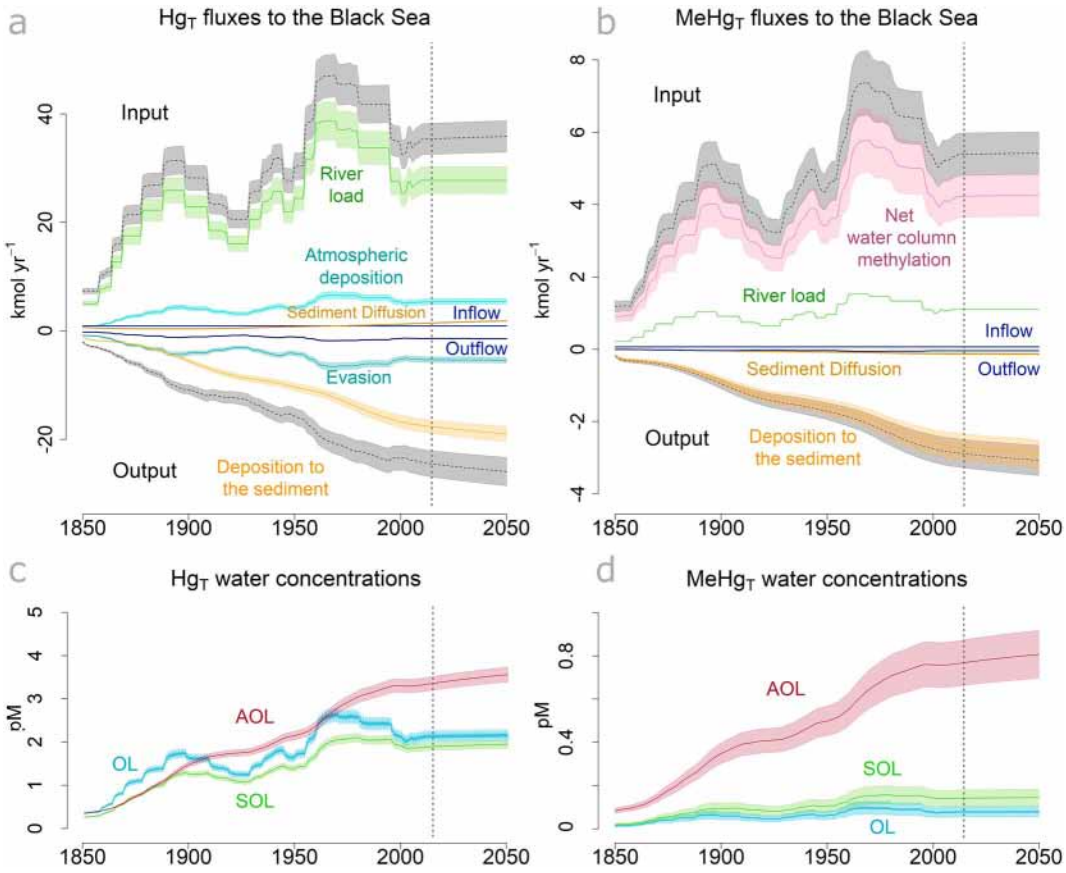

Figure 9. Modeled temporal evolution of (a) Hg_T and (b) MeHg fluxes to the Black Sea after 3 years model spin-up, along with modeled (c) Hg_T and (d) $MeHg_T$ concentrations in the water layers for 1850–2050. The vertical dotted lines indicate the reference year (2013). OL = oxic layer; SOL = suboxic layer; AOL = anoxic layer.

Hg_D in the water column is 1675 ± 320 kmol (~320 ± 64 t), 23% of which (358 ± 49 kmol; ~77 ± 10 t) is present as $MeHg_D$; the mismatch between modeled and measured concentrations for the mean modeled concentrations amounts to ~143 kmol for Hg_D and ~6.8 kmol for $MeHg_D$.

Our budget of Hg_T in the Black Sea (Figures 8 and 9a), built on biogeochemical modeling and measurements along 10 stations, is here compared to the budget of Hg_T estimated by Lamborg et al. (2008) based on water column measurements at two sites in the Black Sea. The highest mismatch between the two budgets is in the estimate of Mediterranean inflow-outflow and Hg^0 evasion. Our estimate of inflow (~0.9 kmol yr^{-1} of Hg_T) and outflow (1.5 ± 0.1 kmol yr^{-1}), based on water column measurements on both sides, implies a small net export of Hg species (~0.6 kmol yr^{-1} of Hg_T) to the Mediterranean Sea, while in the budget of Lamborg et al. (2008) a net input of 5 kmol yr^{-1} is estimated, assuming high concentrations in the Marmara inflow (24 pM) that are not supported by observations. Our estimate of Hg^0 evasion from the water (5.4 ± 0.5 kmol yr^{-1}) is much lower than the 93 kmol yr^{-1} estimated by Lamborg et al. (2008). The concentrations of Hg^0 measured by Lamborg et al. (2008) in surface water (0.3 pM) are slightly higher than the 0.2 pM modeled in our simulation. The evasion rate estimated by Lamborg et al. (2008) and computed by our model (respectively, ~600 pmol m^{-2}d^{-1} and ~50 pmol m^{-2}d^{-1}) lies in the upper and lower range of the rates observed in coastal, shelf, and ocean stations (Andersson et al., 2007; Gårdfeldt et al., 2003; Soerensen et al., 2013). The atmospheric Hg deposition to the Black Sea (5.3 kmol yr^{-1} over the surface area of our model) modeled through the Weather Research and Forecasting Model with Chemistry model is close to the 8 kmol yr^{-1} estimated by Lamborg et al. (2008). The modeled deposition rate (3.6 μg m^{-2} yr^{-1}) is within the range estimated for the Mediterranean Sea (Arctic Monitoring and Assessment Programme/United Nations Environmental Programme, 2013; Gencarelli et al., 2015). The riverine load (24.5 ± 2.5 kmol yr^{-1}) is higher than the 8 kmol yr^{-1} estimated by Lamborg et al. (2008), who acknowledged that the flux was likely higher. The scarcity of observations from the Black Sea tributaries calls for a more thorough investigation. Hg_D diffusion from pore water has a small overall impact on our budget

(1.4 ± 0.1 kmol yr^{-1}) and is lower than, but consistent with, the 4 kmol yr^{-1} predicted by Lamborg et al. (2008), who also included the contribution of shelf sediments.

Our model also simulates the time evolution of MeHg fluxes and concentrations (Figures 9b and 9d); thus, here we provide the first attempt —to the best of or knowledge —to quantify the cycle of this important compound in the Black Sea. For the 2013 MeHg budget (Figure 8), the estimated inputs to the water (~5.2 ± 0.6 kmol yr^{-1}) are larger than the outputs (4.5 ± 0.5 kmol yr^{-1}), and the bulk of MeHg (~3.8 ± 1.3 kmol yr^{-1}) comes from in situ methylation in the AOL. Net MeHg demethylation occurs in the OL (~1.1 kmol yr^{-1}) and SOL (~6.2 kmol yr^{-1}) and net Hg methylation in the AOL (~11.1 kmol y^{-1}). In the OL, 0.1–0.3% of the Hg^{II} pool is methylated and 3–8% of the MeHg pool is demethylated on a daily basis; MeHg has a turnover time of 11–33 d^{-1}. In the SOL, both processes are most efficient: every day 0.7–1.4% of the Hg^{II} pool is demethylated and 9–27% of the MeHg pool is methylated; MeHg has a turnover time of 4–11 d^{-1}. In the AOL, Hg methylation involve 0.1–0.3% of the Hg^{II} pool, and MeHg demethylation 0.4–1% of the MeHg pool; the turnover time of MeHg is 100–240 d^{-1}.

Rivers account for 1.1 kmol yr^{-1} of MeHg (20% of total inputs), while minimal contributions come from the Marmara and Azov Seas, which together account for 1.6% (0.06 and 0.04 kmol yr^{-1}). The diffusion of $MeHg_D$ is predicted to be a sink for the water rather than a source, transferring 0.1 ± 0.01 kmol yr^{-1} to the sediment (3% of outputs). Approximately 4.4 ± 0.6 kmol yr^{-1} of MeHg leaves the water column after settling and deposition, while 0.04 ± 0.01 kmol yr^{-1} moves to the Marmara Sea, transported by the Mediterranean outflow. According to our budget, methylation in the AOL is the most relevant source of MeHg to the basin. Thus, this process needs to be further investigated in the field. Based on the Fe peak in the upper AOL, methylation may be driven by Fe-reducing bacteria, which have been reported to prompt Hg desorption and methylation by using Fe oxides as electron acceptors (Hellal et al., 2015; Kerin et al., 2006; Schaefer et al., 2011; Si et al., 2015), whereas sulfate-reducing bacteria (Benoit et al., 2001; King et al., 2000; Moreau et al., 2015; Schaefer et al., 2014) are likely to contribute significantly to Hg methylation in the lower part of the AOL, where $HS^- > 100$ μM and increases with depth. However, they could also play a role in Hg methylation within aggregates settling from the SOL to the AOL (section 3.1). Large aggregates of precipitates, organic, and inorganic matter that form in the SOL and sink also operate also as carriers of bacteria (Fuchsman et al., 2011). While Hg methylation and MeHg demethylation are thought to involve mainly dissolved Hg species, they have been detected in particles and marine snow aggregates and at particle surfaces under laboratory conditions (Jonsson et al., 2016; Ortiz et al., 2015). It has been proposed that in the Black Sea, all S cycling may occur within the microniches offered by marine snow aggregates (Fuchsman et al., 2011), and Hg methylation may occur within marine snow aggregates formed in the SOL that settle toward the AOL as well as at the surface of FeS and HgS minerals that precipitate in the AOL. Based on the recent identification of new bacterial strains able to methylate Hg (Gilmour et al., 2013), there are other potential candidates for Hg methylation in the AOL of the Black Sea. These are methanogens and the species *Desulfitobacterium metallireducens* (genus *Firmicutes*), which can use either Mn or Fe oxides as electron acceptors (Villemur et al., 2006). Both methanogens and Mn-reducing bacteria are abundant in the water of the lower SOL and in the upper part of the AOL (Fuchsman et al., 2011; Pimenov & Neretin, 2006).

The idea that Hg methylation occurs in the euxinic waters of the Black Sea is in contrast with previous studies, which suggested that methylation is hindered at $HS^- > 10$ μM (Benoit et al., 2001; Benoit, Gilmour, et al., 1999; Benoit, Mason, & Gilmour, 1999; Lamborg et al., 2008). Such inhibition would be due to a shift in inorganic Hg speciation from a neutral complex (HgS^0) to charged species (e.g., $HgHS_2^-$) that cannot diffuse through microbial cell membranes. This implies that bacterial Hg uptake depends on passive diffusion through the cell, while it has been shown that it can be an energy-dependent transport mediated by carrier proteins and favored by some thiols such as cysteine (Schaefer et al., 2011, 2014; Schaefer & Morel, 2009). Many authors have noted that binding and solubility constants used to model the interactions among Hg/sulfide and Hg/DOM are highly uncertain (Drott et al., 2007; Hsu-Kim et al., 2013; Merritt & Amirbahman, 2009; Skyllberg, 2008). Furthermore, as discussed in section 3.1, Hg speciation in the presence of sulfides is affected by DOM composition, which can delay or inhibit the precipitation of $HgS_{(s)}$ and enhance its dissolution. HgS nanoparticles form under these conditions, which are very reactive particles at the surfaces of which Hg methylation occurs (Deonarine & Hsu-Kim, 2009; Gerbig et al., 2011; Hsu-Kim et al., 2013; Jonsson et al., 2012; Kucharzyk et al., 2015; Ravichandran et al., 1998, 1999; Skyllberg, 2008; Slowey, 2010; Waples et al., 2005; Zhang, Kucharzyk, et al., 2014; Zhang

et al., 2012). Beyond the methylation of HgS nanoparticles observed in laboratory experiments, there is evidence that adds weight to the argument for methylation under sulfidic conditions. Coquery et al. (2003) observed maximum levels of $MeHg_D$ in the anoxic water of a tropical reservoir and attributed these to in situ methylation by sulfate-reducing bacteria. Eckley and Hintelmann (2006) detected methylation only under hypoxic-anoxic conditions in a group of seasonally stratified lakes, with maximal rates just below the oxycline that remained elevated to the bottom of the lake (HS^- up to 30 μM). Hollweg et al. (2009) detected Hg methylation in the sediments of the Chesapeake Bay at sulfide levels as high as 100–1,000 μM, though rates were maximal at $HS^- \sim 1$ μM. Merritt and Amirbahman (2008) reported a MeHg maximum with HS^- ranging from 0.5 to 30 μM in the pore water of the Penobscot River Estuary. In the sediment of Passamaquoddy Bay, Sunderland et al. (2006) observed the highest MeHg/Hg ratio in the zone with sulfide levels between 1,300 and 6,000 μM. Moreover, Hg methylation at millimolar levels of sulfides has been detected in sediment samples and in pure cultures of bacteria (Drott et al., 2007; King et al., 2000; Langer et al., 2001).

Some authors have pointed out that the decrease in Hg methylation with depth, frequently observed in pore water and sediment profiles, might be attributable to the limitation of available NOM substrates (electron donors) rather than to increasing sulfide levels (Drott et al., 2007; Merritt & Amirbahman, 2009). This could explain why profiles of MeHg in the Black Sea water column differ from profiles often observed in pore waters and sediments that exhibit surface or subsurface maxima. In the upper part of the AOL, microbial activity is high due to the NOM produced at the lower boundary of the SOL by chemosynthetic bacteria (Pimenov & Neretin, 2006; Yılmaz et al., 2006).

The temporal evolution of Hg_T concentrations (Figure 9c) in the OL and SOL shows a fast response to changes in atmospheric and riverine loadings and follows the seasonal signal of atmospheric Hg deposition. In the AOL, Hg_T concentrations increase more slowly due to the longer times needed for Hg transport to deep water but are almost linear with time, as the net Hg_T flux from the SOL to AOL is larger than the flux from the AOL to sediment (Figure 8). Similarly to Hg_T, $MeHg_T$ tends to increase with time in the AOL (Figure 9d), where it exhibits maximal concentrations. However, the $MeHg_T$ distribution in the water column differs from Hg_T, and throughout the simulation, concentrations are lower in the OL and SOL and highest in the AOL. This is because $MeHg_T$ is much less affected by external loadings and is rather controlled by in situ production and degradation in the water column. The analysis of time evolution highlights that, in spite of a reduction in anthropogenic Hg input since the 1970s (Figures 9a and 9b), the model predicts the retention and accumulation of Hg species in the AOL, likely due to the "Mn shuttle" transportation process described in section 3.1. Briefly, Mn/Fe oxides in the SOL act as a barrier that limits upward diffusion and favors downward transport of Hg species associated with settling oxides, which are reduced and dissolved in the AOL releasing Hg species. In our model, odixe precipitation and dissolution are represented in a simplified fashion by parametrizing the production of POM within the SOL and its degradation in the first AOL sublayer (Text S2 and Figure S3).

The modeled pool of Hg from natural sources in the Black Sea is between 122 and 268 kmol. By difference with our base simulation, anthropogenic Hg is 1,517–1,663 kmol and accounts for 85%–93% of the water Hg pool.

4. Conclusions

During the 2013 GOETRACES MEDBlack cruise, we measured Hg and MeHg concentrations along the stretched redox gradient of the Black Sea water column. The new measurements were integrated into a numerical model to better understand MeHg production, Hg species cycling in the Black Sea, and their temporal evolution. A comparison between observational data and ensembles of simulations was performed to calibrate the model estimating the most likely value for the uncertain model parameters and their errors, as well as the uncertainty in model output due to parameters uncertainty. Such a comparison also allowed us to reject the hypothesis that Hg methylation is limited to the suboxic water of the Black Sea, and rather, it supports the idea that both Hg methylation and MeHg demethylation occur ubiquitously.

Contrary to a previous assessment (Lamborg et al., 2008), we found the highest MeHg concentrations in the permanently anoxic waters of the Black Sea. These new observations, backed with numerical modeling and mass balance calculations, indicate that Hg methylation in anoxic water is likely to be the primary MeHg source to the basin. Our findings offer additional theoretical and empirical support to increasing evidence that Hg can be methylated under sulfidic conditions, when the NOM pool of the system is bioavailable to

bacteria and contains functional groups that may inhibit the precipitation of HgS. MeHg percentages are highest in anoxic waters (up to 57%) and comparable to other open-ocean subsurface maxima in oxic waters.

According to our budget, inputs of Hg species to the Black Sea water column exceed outputs. Inflows and outflows to the Mediterranean Sea, as well as flux from sediment, are slight. The main source of Hg^{II} is river load followed by atmospheric deposition, while MeHg mostly comes from in situ methylation in anoxic waters. Most of the Hg in the Black Sea water column (85–93%) is of anthropogenic origin. During the time span of the simulation (1850–2050), modeled concentrations of Hg and MeHg increase in the deepest layers of the Black Sea (AOL), owing to recycling between suboxic and anoxic water that limits upward diffusion.

Overall, concentrations of Hg species in the Black Sea water column appear to depend on the balance between (1) the amount of Hg_T (mostly Hg^{II}) that enters surface layers, is scavenged, and is transported to the SOL; (2) the recycling of Hg and MeHg between the SOL and AOL, driven by precipitation and dissolution of Mn, which causes increased Hg and MeHg with time; (3) the net production of MeHg in the AOL; and (4) the transport toward the sediment of the particulate fraction, which is the only removal pathway from deep waters and concerns only a small fraction of the total pool.

Results suggest that also in other water bodies, the hypoxic-anoxic conditions induced at the bottom of the water column by summer stratification could promote methylation over areas much larger than previously thought, generating a significant amount of MeHg that would then be advected to the rest of the water column during the subsequent mixing period.

Acknowledgments

Additional information on methods and results can be found in the supporting information; the original data set from the 2013 GEOTRACES MEDBlack can be accessed at the BCO-DMO database http://www.bco-dmo.org/resources. We acknowledge the Dutch funding agency (project: 822.01.015) of the National Science Foundation NWO for funding this work as part of GEOTRACES. This work was supported by the research grant ERC-2010-StG_20091028 from the European Research Council to J. E. S. This work was supported by the RITMARE Flagship Project funded by the Italian Ministry of University and Research to D. M. C. We thank Andrew Margolin for helpful discussions on the cruise data set and the redox layers of the Black Sea. We thank Léa Cabrol for valuable advice on microbiological aspects. We thank Thomas Pichler for accepting G. R. as a visiting student at the University of Bremen.

References

Agapov, S., Korpakova, I., Aleksandrova, Z., Romova, M., Baskakova, T., Matishov, G., et al. (2012). Standard Hydrochemistry. In *Environmental monitoring of the Black Sea: Monitoring and information system for reducing oil pollution*. Black Sea Commission. Contribution Agreement No 07.0203/2008/518960/SUB/D2. Retrieved from http://www.blacksea-commission.org/_publ-KerchReport.asp#_Toc323887562 (last accessed March 14, 2018)

Agirbas, E., Feyzioglu, A. M., & Kopuz, U. (2014). Seasonal changes of phytoplankton chlorophyll a, primary production and their relation in the continental shelf area of the south eastern Black Sea. *Turkish Journal of Fisheries and Aquatic Sciences*, *14*, 713–726. https://doi.org/10.4194/1303-2712-v14

Arctic Monitoring and Assessment Programme/United Nations Environmental Programme (2013). *Technical background report for the Global Mercury Assessment 2013, Oslo*. Geneva, Switzerland: Norway/UNEP Chemicals Branch.

Amos, H. M., Jacob, D. J., Kocman, D., Horowitz, H. M., Zhang, Y., Dutkiewicz, S., et al. (2014). Global biogeochemical implications of mercury discharges from rivers and sediment burial. *Environmental Science & Technology*, *48*(16), 9514–9522. https://doi.org/10.1021/es502134t

Amos, H. M., Sonke, J. E., Obrist, D., Robins, N., Hagan, N., Horowitz, H. M., et al. (2015). Observational and modeling constraints on global anthropogenic enrichment of mercury. *Environmental Science & Technology*, *49*(7), 4036–4047. https://doi.org/10.1021/es5058665

Andersson, M. E., Gårdfeldt, K., Wängberg, I., Sprovieri, F., Pirrone, N., & Lindqvist, O. (2007). Reprint of "Seasonal and daily variation of mercury evasion at coastal and off shore sites from the Mediterranean Sea". *Marine Chemistry*, *107*(1), 104–116. https://doi.org/10.1016/j.marchem.2007.06.020

Balogh, S. J., Huang, Y., Offerman, H. J., Meyer, M. L., & Johnson, D. K. (2003). Methylmercury in rivers draining cultivated watersheds. *Science of the Total Environment*, *304*(1–3), 305–313. https://doi.org/10.1016/S0048-9697(02)00577-6

Beck, M. B. (1987). Water quality modeling: A review of the analysis of uncertainty. *Water Resources Research*, *23*, 1393–1442. https://doi.org/10.1029/WR023i008p01393

Benoit, J. M., Gilmour, C. C., & Mason, R. P. (2001). Aspects of bioavailability of mercury for methylation in pure cultures of Desulfobulbus propionicus (1pr3). *Applied and Environmental Microbiology*, *67*(1), 51–58. https://doi.org/10.1128/AEM.67.1.51-58.2001

Benoit, J. M., Gilmour, C. C., Mason, R. P., & Heyes, A. (1999). Sufide controls on bioavailability to methylating bacteria in sediment pore waters. *Environmental Science & Technology*, *33*(6), 951–957. https://doi.org/10.1021/es9808200

Benoit, J. M., Mason, R. P., & Gilmour, C. C. (1999). Estimation of mercury-sulfide speciation in sediment pore waters using octanol-water partitioning and implications for availability to methylating bacteria. *Environmental Toxicology and Chemistry*, *18*(10), 2138–2141. https://doi.org/10.1002/etc.5620181004

Berlinsky, N., Bogatova, Y., & Garkavaya, G. (2006). Estuary of the Danube. In P. J. Wangersky (Ed.), *Estuaries* (pp. 233–264). Berlin: Springer. https://doi.org/10.1007/698_5_021

Bouchet, S., Amouroux, D., Rodriguez-Gonzalez, P., Tessier, E., Monperrus, M., Thouzeau, G., et al. (2013). MMHg production and export from intertidal sediments to the water column of a tidal lagoon (Arcachon Bay, France). *Biogeochemistry*, *114*(1–3), 341–358. https://doi.org/10.1007/s10533-012-9815-z

Bowman, K. L., Hammerschmidt, C. R., Lamborg, C. H., & Swarr, G. (2015). Mercury in the North Atlantic Ocean: The U.S. GEOTRACES zonal and meridional sections. *Deep Sea Research Part II: Topical Studies in Oceanography*, *116*, 251–261. https://doi.org/10.1016/j.dsr2.2014.07.004

Bowman, K. L., Hammerschmidt, C. R., Lamborg, C. H., Swarr, G. J., & Agather, A. M. (2016). Distribution of mercury species across a zonal section of the eastern tropical South Pacific Ocean (U.S. GEOTRACES GP16). *Marine Chemistry*, *186*, 156–166. https://doi.org/10.1016/j.marchem.2016.09.005

Bravo, A. G., Bouchet, S., Tolu, J., Björn, E., Mateos-Rivera, A., & Bertilsson, S. (2017). Molecular composition of organic matter controls methylmercury formation in boreal lakes. *Nature Communications*, *8*, 1–9. https://doi.org/10.1038/ncomms14255

Canu, D., & Rosati, G. (2017). Long-term scenarios of mercury budgeting and exports for a Mediterranean hot spot (Marano-Grado Lagoon, Adriatic Sea). *Estuarine, Coastal and Shelf Science*, 1–11. https://doi.org/10.1016/j.ecss.2016.12.005

Chasovnikov, V., Nasurov, A., Korshenko, A., Ermakov, V., Zhugailo, S., Eremeev, V., et al. (2012). Other Pollutants in the Kerch Strait. In *Environmental monitoring of the Black Sea: Monitoring and information system for reducing oil pollution*. Black Sea Commission. Contribution Agreement No 07.0203/2008/518960/SUB/D2. http://www.blacksea-commission.org/_publ-KerchReport.asp#_Toc323887562 (last accessed March 14, 2018)

Clarkson, T. W., & Magos, L. (2006). The toxicology of mercury and its chemical compounds. *Critical Reviews in Toxicology*, *36*(8), 609–662. https://doi.org/10.1080/10408440600845619

Çoban-Yıldız, Y., Altabet, M. A., Yılmaz, A., & Tuğrul, S. (2006). Carbon and nitrogen isotopic ratios of suspended particulate organic matter (SPOM) in the Black Sea water column. *Deep Sea Research Part II: Topical Studies in Oceanography*, *53*(17-19), 1875–1892. https://doi.org/10.1016/j.dsr2.2006.03.021

Çoban-Yıldız, Y., Tugrul, S., Ediger, D., Yilmaz, A., & Polat, S. C. (2000). A comparative study on the abundance and elemental composition of POM in three interconnected basins: The Black, the Marmara and the Mediterranean Seas. *Mediterranean Marine Science*, *1*(1), 51–63. https://doi.org/10.12681/mms.5

Coquery, M., Cossa, D., Peretyazhko, T., Azemard, S., & Charlet, L. (2003). Methylmercury formation in the anoxic waters of the Petit-Saut reservoir (French Guiana) and its spreading in the adjacent Sinnamary river. *Jounal Physique IV*, *107*(1999), 327–331. https://doi.org/10.1051/jp4:20030308

Cossa, D., Averty, B., & Pirrone, N. (2009). The origin of methylmercury in open Mediterranean waters. *Limnology and Oceanography*, *54*(3), 837–844. https://doi.org/10.4319/lo.2009.54.3.0837

Cossa, D., & Coquery, M. (2005). The mediterranean mercury anomaly, a geochemical or a biological issue. In A. Saliot (Ed.), *The Mediterranean Sea* (pp. 177–208). Berlin: Springer. https://doi.org/10.1007/b107147

Cossa, D., Garnier, C., Buscail, R., Elbaz-Poulichet, N., Mikac, F., Patel-Sorrentino, E., et al. (2014). A Michaelis–Menten type equation for describing methylmercury dependence on inorganic mercury in aquatic sediments. *Biogeochemistry*, *119*(1-3), 35–43. https://doi.org/10.1007/s10533-013-9924-3

Cossa, D., Harmelin-Vivien, M., Mellon-Duval, C., Loizeau, V., Averty, B., Crochet, S., et al. (2012). Influences of bioavailability, trophic position, and growth on methylmercury in hakes (*Merluccius merluccius*) from Northwestern Mediterranean and Northeastern Atlantic. *Environmental Science & Technology*, *46*(9), 4885–4893. https://doi.org/10.1021/es204269w

Cossa, D., Heimbürger, L. E., Lannuzel, D., Rintoul, S. R., Butler, E. C. V., Bowie, A. R., et al. (2011). Mercury in the Southern Ocean. *Geochimica et Cosmochimica Acta*, *75*(14), 4037–4052. https://doi.org/10.1016/j.gca.2011.05.001

Cossarini, G., & Solidoro, C. (2008). Global sensitivity analysis of a trophodynamci model of the Gulf of Trieste. *Ecological Modelling*, *212*(1–2), 16–27. https://doi.org/10.1016/j.ecolmodel.2007.10.009

De Baar, H. J. W., Timmermans, K. R., Laan, P., De Porto, H. H., Ober, S., Blom, J. J., et al. (2008). Titan: A new facility for ultraclean sampling of trace elements and isotopes in the deep oceans in the international Geotraces program. *Marine Chemistry*, *111*(1-2), 4–21. https://doi.org/10.1016/j.marchem.2007.07.009

De Simone, F., Gencarelli, C. N., Hedgecock, I. M., & Pirrone, N. (2014). Global atmospheric cycle of mercury: A model study on the impact of oxidation mechanisms. *Environmental Science and Pollution Research*, *21*(6), 4110–4123. https://doi.org/10.1007/s11356-013-2451-x

De Simone, F., Gencarelli, C. N., Hedgecock, I. M., & Pirrone, N. (2016). A modeling comparison of mercury deposition from current anthropogenic mercury emission inventories. *Environmental Science & Technology*, *50*(10), 5154–5162. https://doi.org/10.1021/acs.est.6b00691

Dellwig, O., Leipe, T., März, C., Glockzin, M., Pollehne, F., Schnetger, B., et al. (2010). A new particulate Mn–Fe–P-shuttle at the redoxcline of anoxic basins. *Geochimica et Cosmochimica Acta*, *74*(24), 7100–7115. https://doi.org/10.1016/j.gca.2010.09.017

Deonarine, A., & Hsu-Kim, H. (2009). Precipitation of mercuric sulfide nanoparticles in NOM-containing water: Implications for the natural environment. *Environmental Science & Technology*, *43*(7), 2368–2373. https://doi.org/10.1021/es803130h

Deuser, W. G. (1971). Organic-carbon budget of the Black Sea. *Deep Sea Research and Oceanographic Abstracts*, *18*(10), 995–1004. https://doi.org/10.1016/0011-7471(71)90004-0

Drott, A., Lambertsson, L., Björn, E., & Skyllberg, U. (2007). Importance of dissolved neutral mercury sulfides for methyl mercury production in contaminated sediments. *Environmental Science & Technology*, *41*(7), 2270–2276. https://doi.org/10.1021/es061724z

Ducklow, H. W., Hansell, D. A., & Morgan, J. A. (2007). Dissolved organic carbon and nitrogen in the western Black Sea. *Marine Chemistry*, *105*(1–2), 140–150. https://doi.org/10.1016/j.marchem.2007.01.015

Eckley, C. S., & Hintelmann, H. (2006). Determination of mercury methylation potentials in the water column of lakes across Canada. *Science of the Total Environment*, *368*(1), 111–125. https://doi.org/10.1016/j.scitotenv.2005.09.042

Emmons, L. K., Walters, S., Hess, P. G., Lamarque, J. F., Pfister, G. G., Fillmore, D., et al. (2010). Description and evaluation of the Model for Ozone and Related chemical Tracers, version 4 (MOZART-4). *Geoscientific Model Development*, *3*(1), 43–67. https://doi.org/10.5194/gmd-3-43-2010

Fantozzi, L., Manca, G., Ammoscato, I., Pirrone, N., & Sprovieri, F. (2013). The cycling and sea-air exchange of mercury in the waters of the Eastern Mediterranean during the 2010 MED-OCEANOR cruise campaign. *Science of the Total Environment*, *448*, 151–162. https://doi.org/10.1016/j.scitotenv.2012.09.062

Fitzgerald, W. F., Lamborg, C. H., & Hammerschmidt, C. R. (2007). Marine biogeochemical cycling of mercury marine biogeochemical cycling of mercury. *Public Health*, *107*, 641–662. https://doi.org/10.1021/cr050353m

Froelich, P. N., Klinkhammer, G. P., Bender, M. L., Luedtke, N. A., Heath, G. R., Cullen, D., et al. (1979). Early oxidation of organic matter in pelagic sediments of the eastern equatorial Atlantic: Suboxic diagenesis. *Geochimica et Cosmochimica Acta*, *43*(7), 1075–1090. https://doi.org/10.1016/0016-7037(79)90095-4

Fuchsman, C. A., Kirkpatrick, J. B., Brazelton, W. J., Murray, J. W., & Staley, J. T. (2011). Metabolic strategies of free-living and aggregate-associated bacterial communities inferred from biologic and chemical profiles in the Black Sea suboxic zone. *FEMS Microbiology Ecology*, *78*(3), 586–603. https://doi.org/10.1111/j.1574-6941.2011.01189.x

Ganachaud, A., Cravatte, S., Sprintall, J., Germineaud, C., Alberty, M., Jeandel, C., et al. (2017). The Solomon Sea: Its circulation, chemistry, geochemistry and biology explored during two oceanographic cruises. *Elementa: Science of the Anthropocene*, *5*(0), 33. https://doi.org/10.1525/elementa.221

Gårdfeldt, K., Sommar, J., Ferrara, R., Ceccarini, C., Lanzillotta, E., Munthe, J., et al. (2003). Evasion of mercury from coastal and open waters of the Atlantic Ocean and the Mediterranean Sea. *Atmospheric Environment*, *37*, 73–84. https://doi.org/10.1016/S1352-2310(03)00238-3

Gencarelli, C. N., Bieser, J., Carbone, F., De Simone, F., Hedgecock, I. M., Matthias, V., et al. (2017). Sensitivity model study of regional mercury dispersion in the atmosphere. *Atmospheric Chemistry and Physics Discussions*, *17*, 1–24. https://doi.org/10.5194/acp-2016-663

Gencarelli, C. N., De Simone, F., Hedgecock, I. M., Sprovieri, F., & Pirrone, N. (2014). Development and application of a regional-scale atmospheric mercury model based on WRF/Chem: A Mediterranean area investigation. *Environmental Science and Pollution Research*, *21*(6), 4095–4109. https://doi.org/10.1007/s11356-013-2162-3

Gencarelli, C. N., De Simone, F., Hedgecock, I. M., Sprovieri, F., Yang, X., & Pirrone, N. (2015). European and Mediterranean mercury modelling: Local and long-range contributions to the deposition flux. *Atmospheric Environment*, *117*, 162–168. https://doi.org/10.1016/j.atmosenv.2015.07.015

Gerbig, C. A., Kim, C. S., Stegemeier, J. P., Ryan, J. N., & Aiken, G. R. (2011). Formation of nanocolloidal metacinnabar in mercury-DOM-sulfide systems. *Environmental Science & Technology*, *45*(21), 9180–9187. https://doi.org/10.1021/es201837h

Gerringa, L. J. A., Rijkenberg, M. J. A., Bown, J., Margolin, A. R., Laan, P., & de Baar, H. J. W. (2016). Fe-binding dissolved organic ligands in the oxic and suboxic waters of the Black Sea. *Frontiers in Marine Science*, *3*, 84.

Gilmour, C. C., Podar, M., Bullock, A. L., Graham, A. M., Brown, S. D., Somenahally, A. C., et al. (2013). Mercury methylation by novel microorganisms from new environments. *Environmental Science & Technology*, *47*(20), 11810–11820. https://doi.org/10.1021/es403075t

Graham, A. M., Aiken, G. R., & Gilmour, C. C. (2012). Dissolved organic matter enhances microbial mercury methylation under sulfidic conditions. *Environmental Science and Technology*, *46*(5), 2715–2723. https://doi.org/10.1021/es203658f

Grégoire, M., & Soetaert, K. (2010). Carbon, nitrogen, oxygen and sulfide budgets in the Black Sea: A biogeochemical model of the whole water column coupling the oxic and anoxic parts. *Ecological Modelling*, *221*(19), 2287–2301. https://doi.org/10.1016/j.ecolmodel.2010.06.007

Grell, G. A., Peckham, S. E., Schmitz, R., McKeen, S. A., Frost, G., Skamarock, W. C., & Eder, B. (2005). Fully coupled "online" chemistry within the WRF model. *Atmospheric Environment*, *39*(37), 6957–6975. https://doi.org/10.1016/j.atmosenv.2005.04.027

Hammerschmidt, C. R., & Bowman, K. L. (2012). Vertical methylmercury distribution in the subtropical North Pacific Ocean. *Marine Chemistry*, *132-133*, 77–82. https://doi.org/10.1016/j.marchem.2012.02.005

Hammerschmidt, C. R., & Fitzgerald, W. F. (2006). Bioaccumulation and trophic transfer of methylmercury in Long Island Sound. *Archives of Environmental Contamination and Toxicology*, *51*(3), 416–424. https://doi.org/10.1007/s00244-005-0265-7

Hammerschmidt, C. R., Fitzgerald, W. F., Lamborg, C. H., Balcom, P. H., & Visscher, P. T. (2004). Biogeochemistry of methylmercury in sediments of Long Island Sound. *Marine Chemistry*, *90*(1-4), 31–52. https://doi.org/10.1016/j.marchem.2004.02.024

Han, S., Lehman, R. D., Choe, K.-Y., & Gill, G. A. (2007). Chemical and physical speciation of mercury in Offatts Bayou: A seasonally anoxic bayou in Galveston Bay. *Limnology and Oceanography*, *52*(4), 1380–1392. https://doi.org/10.4319/lo.2007.52.4.1380

Han, S., Obraztsova, A., Pretto, P., Choe, K.-Y., Gieskes, J., Deheyn, D. D., & Tebot, B. M. (2007). Biogeochemical factors affecting mercury methylation in sediments of the Venice Lagoon, Italy. *Environmental Toxicology and Chemistry*, *26*(4), 655–663. https://doi.org/10.1897/06-392R.1

Heimbürger, L.-E., Cossa, D., Marty, J.-C., Migon, C., Averty, B., Dufour, A., & Ras, J. (2010). Methyl mercury distributions in relation to the presence of nano- and picophytoplankton in an oceanic water column (Ligurian Sea, North-western Mediterranean). *Geochimica et Cosmochimica Acta*, *74*(19), 5549–5559. https://doi.org/10.1016/j.gca.2010.06.036

Heimbürger, L.-E., Sonke, J. E., Cossa, D., Point, D., Lagane, C., Laffont, L., et al. (2015). Shallow methylmercury production in the marginal sea ice zone of the central Arctic Ocean. *Scientific Reports*, *5*(1), 10318. https://doi.org/10.1038/srep10318

Hellal, J., Guédron, S., Huguet, L., Schäfer, J., Laperche, V., Joulian, C., et al. (2015). Mercury mobilization and speciation linked to bacterial iron oxide and sulfate reduction: A column study to mimic reactive transfer in an anoxic aquifer. *Journal of Contaminant Hydrology*, *180*, 56–68. https://doi.org/10.1016/j.jconhyd.2015.08.001

Heyes, A., Mason, R. P., Kim, E. H., & Sunderland, E. (2006). Mercury methylation in estuaries: Insights from using measuring rates using stable mercury isotopes. *Marine Chemistry*, *102*(1–2), 134–147. https://doi.org/10.1016/j.marchem.2005.09.018

Hollweg, T. A., Gilmour, C. C., & Mason, R. P. (2009). Methylmercury production in sediments of Chesapeake Bay and the mid-Atlantic continental margin. *Marine Chemistry*, *114*(3–4), 86–101. https://doi.org/10.1016/j.marchem.2009.04.004

Hollweg, T. A., Gilmour, C. C., & Mason, R. P. (2010). Mercury and methylmercury cycling in sediments of the mid-Atlantic continental shelf and slope. *Limnology and Oceanography*, *55*(6), 2703–2722. https://doi.org/10.4319/lo.2010.55.6.2703

Horowitz, H. M., Jacob, D. J., Amos, H. M., Streets, D. G., & Sunderland, E. M. (2014). Historical mercury releases from commercial products: Global environmental implications. *Environmental Science & Technology*, *48*, 10,242–10,250. https://doi.org/10.1021/es501337j

Hsu-Kim, H., Kucharzyk, K. H., Zhang, T., & Deshusses, M. A. (2013). Mechanisms regulating mercury bioavailability for methylating microorganisms in the aquatic environment: A critical review. *Environmental Science & Technology*, *47*(6), 2441–2456. https://doi.org/10.1021/es304370g

Huerta-Diaz, M. A., & Morse, J. W. (1992). Pyritization of trace metals in anoxic marine sediments. *Geochimica et Cosmochimica Acta*, *56*(7), 2681–2702. https://doi.org/10.1016/0016-7037(92)90353-K

Jaoshvili, S. (2002). In I. Khomerki, G. Gigineishvili, & A. Kordzadze (Eds.), *The rivers of the Black Sea. EEA Technical report 71*(58 pp.). European Environment Agency. Retrieved from https://www.eea.europa.eu/publications/technical_report_2002_71, (last accessed March 14, 2018).

Jonsson, S., N. M. Mazrui, and R. P. Mason (2016). Dimethylmercury formation mediated by inorganic and organic reduced sulfur surfaces, *Scientific Reports*, *6*(1), 27958. https://doi.org/10.1038/srep27958

Jonsson, S., Skyllberg, U., Nilsson, M. B., Westlund, P., Shchukarev, A., Lundberg, E., & Björn, E. (2012). Mercury methylation rates for geochemically relevant HgII species in sediments. *Environmental Science & Technology*, *46*(21), 11,653–11,659. https://doi.org/10.1021/es3015327

Jørgensen, S. E. (1994). *Fundamentals of ecological modelling: Applications in environmental management and research, developments in environmental modelling* (2nd ed.). Amsterdam: Elsevier Science.

Jung, G., Hedgecock, I. M., & Pirrone, N. (2009). Model development ECHMERIT V1. 0—A new global fully coupled mercury-chemistry and transport model. *Geoscientific Model Development*, *2*(2), 175–195. https://doi.org/10.5194/gmd-2-175-2009

Karageorgis, A. P., Gardner, W. D., Georgopoulos, D., Mishonov, A. V., Krasakopoulou, E., & Anagnostou, C. (2008). Particle dynamics in the Eastern Mediterranean Sea: A synthesis based on light transmission, PMC, and POC archives (1991-2001). *Deep Sea Research Part I: Oceanographic Research Papers*, *55*(2), 177–202. https://doi.org/10.1016/j.dsr.2007.11.002

Karageorgis, A. P., Kourafalou, V. H., Anagnostou, C., Tsiaras, K. P., Raitsos, D. E., Papadopoulos, V., & Papadopoulos, A. (2009). River-induced particle distribution in the northwestern Black Sea (September 2002 and 2004). *Journal of Geophysical Research*, *114*, C12003. https://doi.org/10.1029/2009JC005460

Kerin, E. J., Gilmour, C. C., Roden, E., Suzuki, M. T., Coates, J. D., & Mason, R. P. (2006). Mercury methylation by dissimilatory iron-reducing bacteria. *Applied and Environmental Microbiology*, *72*(12), 7919–7921. https://doi.org/10.1128/AEM.01602-06

Kim, H., Soerensen, A. L., Hur, J., Heimbürger, L.-E., Hahm, D., Rhee, T. S., et al. (2017). Methylmercury mass budgets and distribution characteristics in the western Pacific Ocean. *Environmental Science & Technology*, *51*(3), 1186–1194. https://doi.org/10.1021/acs.est.6b04238

King, J. K., Kostka, J. E., Frischer, M. E., & Saunders, M. (2000). Sulfate-reducing bacteria methylate mercury at variable rates in pure culture and in marine sediments. *Applied and Environmental Microbiology*, *66*(6), 2430–2437. https://doi.org/10.1128/AEM.66.6.2430-2437.2000. Updated

Konovalov, S., Samodurov, A., Oguz, T., & Ivanov, L. (2004). Parameterization of iron and manganese cycling in the Black Sea suboxic and anoxic environment. *Deep Sea Research Part I: Oceanographic Research Papers*, *51*(12), 2027–2045. https://doi.org/10.1016/j.dsr.2004.08.005

Konovalov, S., Tuğrul, S., Baştürk, Ö., & Salihoğlu, İ. (1997). Spatial isopycnal analysis of the main pycnocline chemistry of the Black Sea: Seasonal and interannual variations. In E. Özsoy & A. Mikaelyan (Eds.), *Sensitivity to change: Black Sea, Baltic Sea and North Sea* (pp. 197–210). Dordrecht, Netherlands: Springer. https://doi.org/10.1007/978-94-011-5758-2_16

Konovalov, S. K., & Murray, J. W. (2001). Variations in the chemistry of the Black Sea on a time scale of decades (1960–1995). *Journal of Marine Systems*, *31*(1–3), 217–243. https://doi.org/10.1016/S0924-7963(01)00054-9

Kotnik, J., Horvat, M., Ogrinc, N., Fajon, V., Žagar, D., Cossa, D., et al. (2015). Mercury speciation in the Adriatic Sea. *Marine Pollution Bulletin*, *96*(1–2), 136–148. https://doi.org/10.1016/j.marpolbul.2015.05.037

Kucharzyk, K. H., Deshusses, M. A., Porter, K. A., & Hsu-Kim, H. (2015). Relative contributions of mercury bioavailability and microbial growth rate on net methylmercury production by anaerobic mixed cultures. *Environmental Science: Processes and Impacts*, *17*(9), 1568–1577. https://doi.org/10.1039/C5EM00174A

Lamborg, C. H., C. R. Hammerschmidt, and K. L. Bowman (2016), An examination of the role of particles in oceanic mercury cycling, *Philosophical Transactions of the Royal Society A - Mathematical Physical and Engineering Sciences*, *374*(2081), 20150297. https://doi.org/10.1098/rsta.2015.0297

Lamborg, C. H., Yiğiterhan, O., Fitzgerald, W. F., Balcom, P. H., Hammerschmidt, C. R., & Murray, J. (2008). Vertical distribution of mercury species at two sites in the western Black Sea. *Marine Chemistry*, *111*(1-2), 77–89. https://doi.org/10.1016/j.marchem.2007.01.011

Langer, C. S., Fitzgerald, W. F., Visscher, P. T., & Vandal, G. M. (2001). Biogeochemical cycling of methylmercury at Barn Island SaltMarsh, Stonington, CT, USA. *Wetlands Ecology and Management*, *9*(4), 295–310.

Lehnherr, I., Louis, V. L. S., Hintelmann, H., & Kirk, J. L. (2011). Methylation of inorganic mercury in polar marine waters. *Nature Geoscience*, *4*(5), 298–302. https://doi.org/10.1038/ngeo1134

Lin, C.-J., Pongprueksa, P., Lindberg, S. E., Pehkonen, S. O., Byun, D., & Jang, C. (2006). Scientific uncertainties in atmospheric mercury models I: Model science evaluation. *Atmospheric Environment*, *40*(16), 2911–2928. https://doi.org/10.1016/j.atmosenv.2006.01.009

Liu, B., Schaider, L. A., Mason, R. P., Shine, J. P., Rabalais, N. N., & Senn, D. B. (2015). Controls on methylmercury accumulation in northern Gulf of Mexico sediments. *Estuarine, Coastal and Shelf Science*, *159*, 50–59. https://doi.org/10.1016/j.ecss.2015.03.030

Margolin, A. R., Gerringa, L. J. A., Hansell, D. A., & Rijkenberg, M. J. A. (2016). Net removal of dissolved organic carbon in the anoxic waters of the Black Sea. *Marine Chemistry*, *183*, 13–24. https://doi.org/10.1016/j.marchem.2016.05.003

Mason, R. P., Choi, A. L., Fitzgerald, W. F., Hammerschmidt, C. R., Lamborg, C. H., Soerensen, A. L., & Sunderland, E. M. (2012). Mercury biogeochemical cycling in the ocean and policy implications. *Environmental Research*, *119*, 101–117. https://doi.org/10.1016/j.envres.2012.03.013

Mason, R. P., & Fitzgerald, W. F. (1990). Alkylmercury species in the equatorial Pacific. *Nature*, *347*(6292), 457–459. https://doi.org/10.1038/347457a0

Mason, R. P., Fitzgerald, W. F., Hurley, J., Hanson, A. K., Donaghay, P. L., & Sieburth, J. M. (1993). Mercury biogeochemical cycling in a stratified estuary. *Limnology and Oceanography*, *38*(6), 1227–1241. https://doi.org/10.4319/lo.1993.38.6.1227

Melaku Canu, D., Rosati, G., Solidoro, C., Heimbürger, L.-E., & Acquavita, A. (2015). A comprehensive assessment of the mercury budget in the Marano–Grado Lagoon (Adriatic Sea) using a combined observational modeling approach. *Marine Chemistry*, *177*, 742–752. https://doi.org/10.1016/j.marchem.2015.10.013

Merritt, K. A., & Amirbahman, A. (2008). Methylmercury cycling in estuarine sediment pore waters (Penobscot River estuary, Maine, USA). *Limnology and Oceanography*, *53*(3), 1064–1075. https://doi.org/10.4319/lo.2008.53.3.1064

Merritt, K. A., & Amirbahman, A. (2009). Mercury methylation dynamics in estuarine and coastal marine environments—A critical review. *Earth-Science Reviews*, *96*(1–2), 54–66. https://doi.org/10.1016/j.earscirev.2009.06.002

Monperrus, M., Tessier, E., Amouroux, D., Leynaert, A., Huonnic, P., & Donard, O. F. X. (2007). Mercury methylation, demethylation and reduction rates in coastal and marine surface waters of the Mediterranean Sea. *Marine Chemistry*, *107*(1), 49–63. https://doi.org/10.1016/j.marchem.2007.01.018

Monperrus, M., Tessier, E., Point, D., Vidimova, K., Amouroux, D., Guyoneaud, R., et al. (2007). The biogeochemistry of mercury at the sediment-water interface in the Thau Lagoon. 2. Evaluation of mercury methylation potential in both surface sediment and the water column. *Estuarine, Coastal and Shelf Science*, *72*(3), 485–496. https://doi.org/10.1016/j.ecss.2006.11.014

Moreau, J. W., Gionfriddo, C. M., Krabbenhoft, D. P., Ogorek, J. M., DeWild, J. F., Aiken, G. R., & Roden, E. E. (2015). The effect of natural organic matter on mercury methylation by desulfobulbus propionicus 1pr3. *Frontiers in Microbiology*, *6*, 1389. https://doi.org/10.3389/fmicb.2015.01389

Morel, F. M. M., Kraepiel, A. M. L., & Amyot, M. (1998). The chemical cycle and bioaccumulation of mercury. *Annual Review of Ecology and Systematics*, *29*(1), 543–566. https://doi.org/10.1146/annurev.ecolsys.29.1.543

Morse, J. W., & Luther, G. W. (1999). Chemical influences on trace metal-sulfide interactions in anoxic sediments. *Geochimica et Cosmochimica Acta*, *63*(19-20), 3373–3378. https://doi.org/10.1016/S0016-7037(99)00258-6

Munson, K. M., Lamborg, C., Swarr, G. J., & Saito, M. A. (2015). Mercury species concentrations and fluxes in the central tropical Pacific Ocean. *Global Biogeochemical Cycles*, *29*, 656–676. https://doi.org/10.1002/2015GB005120

Muresan, B., Cossa, D., Jezequel, D., Prévot, F., & Kerbellec, S. (2007). The biogeochemistry of mercury at the sediment-water interface in the Thau lagoon. 1. Partition and speciation. *Estuarine, Coastal and Shelf Science*, *72*(3), 472–484. https://doi.org/10.1016/j.ecss.2006.11.015

Murray, J. W., Stewart, K., Kassakian, S., Krynytzky, M., & Dijulio, D. (2007). Oxic, suboxic, and anoxic conditions in the Black Sea. In *The Black Sea flood question: Changes in coastline, climate, and human settlement* (pp. 1–21). Dordrecht: Springer.

Neretin, L. N., Pohl, C., Jost, G., Leipe, T., & Pollehne, F. (2003). Manganese cycling in the Gotland Deep, Baltic Sea. *Marine Chemistry*, *82*(3–4), 125–143. https://doi.org/10.1016/S0304-4203(03)00048-3

Neu, J. L., & Prather, M. J. (2012). Toward a more physical representation of precipitation scavenging in global chemistry models: Cloud overlap and ice physics and their impact on tropospheric ozone. *Atmospheric Chemistry and Physics*, *12*(7), 3289–3310. https://doi.org/10.5194/acp-12-3289-2012

Nyffeler, F., Godet, C. H., Kontar, E., Kos, R., & Krivosheya, V. G. (2007). Optical properties of the water column along the continental margin of the North Eastern Black Sea. *Journal of Marine Systems*, *31*, 35–44.

Oguz, T., Ducklow, H. W., & Malanotte-Rizzoli, P. (2000). Modeling distinct vertical biogeochemical structure of the black sea: Dynamical coupling of the oxic, suboxic, and anoxic layers. *Global Biogeochemical Cycles*, *14*(4), 1331–1352. https://doi.org/10.1029/1999GB001253

Oken, E., Choi, A. L., Karagas, M. R., Mariën, K., Rheinberger, C. M., Schoeny, R., et al. (2012). Which fish should I eat? Perspectives influencing fish consumption choices. *Environmental Health Perspectives*, *120*(6), 790–798. https://doi.org/10.1289/ehp.1104500

Ortiz, V. L., Mason, R. P., & Evan Ward, J. (2015). An examination of the factors influencing mercury and methylmercury particulate distributions, methylation and demethylation rates in laboratory-generated marine snow. *Marine Chemistry*, *177*(Pt 5), 753–762. https://doi.org/10.1016/j.marchem.2015.07.006

Ovsienko, S., Fashchuk, D., Zatsepa, S., Ivchenko, A., Petrenko, O., Ilyin, Y., et al. (2012). Background hydro-meteorological conditions of the Kerch Strait area. In Black Sea Commission (Ed.), *Environmental monitoring of the Black Sea: Monitoring and information system for reducing oil pollution*. Black Sea Commission. Contribution Agreement No 07.0203/2008/518960/SUB/D2. Retrieved from http://www.blacksea-commission.org/_publ-KerchReport.asp#_Toc323887562, (last accessed March 14, 2018)

Özsoy, E., & Ünlüata, Ü. (1997). Oceanography of the Black Sea: A review of some recent results. *Earth-Science Reviews*, *42*(4), 231–272. https://doi.org/10.1016/S0012-8252(97)81859-4

Pakhomova, S., & Yakushev, E. V. (2013). Manganese and iron at the redox interfaces in the Black Sea, the Baltic Sea, and the Oslo Fjord. In E. V. Yakushev (Ed.), *Chemical structure of pelagic redox interfaces SE - 98* (Vol. 22, pp. 67–93). Berlin: Springer.

Paller, M. H., Jagoe, C. H., Bennett, H., Brant, H. A., & Bowers, J. A. (2004). Influence of methylmercury from tributary streams on mercury levels in Savannah River Asiatic clams. *Science of the Total Environment*, *325*(1–3), 209–219. https://doi.org/10.1016/j.scitotenv.2003.11.008

Panin, N., & Jipa, D. (2002). Danube river sediment input and its interaction with the North-western Black Sea. *Estuarine, Coastal and Shelf Science*, *54*(3), 551–562. https://doi.org/10.1006/ecss.2000.0664

Pianosi, F., Beven, K., Freer, J., Hall, J. W., Rougier, J., Stephenson, D. B., & Wagener, T. (2016). Environmental modelling & software sensitivity analysis of environmental models: A systematic review with practical work flow. *Environmental Modelling and Software*, *79*, 214–232. https://doi.org/10.1016/j.envsoft.2016.02.008

Pimenov, N. V., & Neretin, L. N. (2006). Composition and activities of microbial communities involved in carbon, sulfur, nitrogen and manganese cycling in the oxic/anoxic interface of the Black Sea. In L. N. Neretin (Ed.), *Past and present water column anoxia* (pp. 501–521). Dordrecht, Netherlands: Springer. https://doi.org/10.1007/1-4020-4297-3

Ravichandran, M., Aiken, G. R., Reddy, M. M., & Ryan, J. N. (1998). Enhanced dissolution of cinnabar (mercuric sulfide) by dissolved organic matter isolated from the Florida Everglades. *Environmental Science & Technology*, *32*(21), 3305–3311. https://doi.org/10.1021/es9804058

Ravichandran, M., Aiken, G. R., Ryan, J. N., & Reddy, M. M. (1999). Inhibition of precipitation and aggregation of metacinnabar (HgS) by humic substances isolated from the Florida Everglades. *Abstracts of Papers American Chemical Society*, 217(9), 105–ENVR. https://doi.org/10.1021/es9811187

Rodríguez Martín-Doimeadios, R. C., Tessier, E., Amouroux, D., Guyoneaud, R., Duran, R., Caumette, P., & Donard, O. F. X. (2004). Mercury methylation/demethylation and volatilization pathways in estuarine sediment slurries using species-specific enriched stable isotopes. *Marine Chemistry*, *90*(1–4), 107–123. https://doi.org/10.1016/j.marchem.2004.02.022

Salzmann, M., & Lawrence, M. G. (2006). Automatic coding of chemistry solvers in WRF-Chem using KPP. *7th WRF User's Workshop*, Boulder, CO.

Sandu, A., & Sander, R. (2006). Technical note: Simulating chemical systems in Fortran90 and Matlab with the Kinetic PreProcessor KPP-2.1. *Atmospheric Chemistry and Physics*, *6*(1), 187–195. https://doi.org/10.5194/acp-6-187-2006

Schaefer, J. K., & Morel, F. M. M. (2009). High methylation rates of mercury bound to cysteine by Geobacter sulfurreducens. *Nature Geoscience*, *2*(2), 123–126.

Schaefer, J. K., Rocks, S. S., Zheng, W., Liang, L., Gu, B., Morel, F. M. M. M., et al. (2011). Active transport, substrate specificity, and methylation of Hg(II) in anaerobic bacteria. *Proceedings of the National Academy of Sciences of the United States of America*, *108*(21), 8714–8719. https://doi.org/10.1073/pnas.1105781108

Schaefer, J. K., Szczuka, A., & Morel, F. M. M. (2014). Effect of divalent metals on Hg(II) uptake and methylation by bacteria. *Environmental Science & Technology*, *48*(5), 3007–3013. https://doi.org/10.1021/es405215v

Schartup, A. T., Balcom, P. H., & Mason, R. P. (2014). Sediment-porewater partitioning, total sulfur, and methylmercury production in estuaries. *Environmental Science & Technology*, *48*(2), 954–960. https://doi.org/10.1021/es403030d

Schartup, A. T., Balcom, P. H., Soerensen, A. L., Gosnell, K. J., Calder, R. S. D., Mason, R. P., & Sunderland, E. M. (2015). Freshwater discharges drive high levels of methylmercury in Arctic marine biota. *Proceedings of the National Academy of Sciences*, *112*(38), 11,789–11,794. https://doi.org/10.1073/pnas.1505541112

Schartup, A. T., Mason, R. P., Balcom, P. H., Hollweg, T. A., & Chen, C. Y. (2013). Methylmercury production in estuarine sediments: Role of organic matter. *Environmental Science & Technology*, *47*(2), 695–700. https://doi.org/10.1021/es302566w

Schartup, A. T., Ndu, U., Balcom, P. H., Mason, R. P., & Sunderland, E. M. (2015). Contrasting effects of marine and terrestrially derived dissolved organic matter on mercury speciation and bioavailability in seawater. *Environmental Science & Technology*, *49*(10), 5965–5972. https://doi.org/10.1021/es506274x

Schijf, J., de Baar, H. J. W., Wijbrans, J. R., & Landing, W. M. (1991). Dissolved rare earth elements in the Black Sea. *Deep Sea Research Part A. Oceanographic Research Papers*, *38*, S805–S823. https://doi.org/10.1016/S0198-0149(10)80010-X

Schlitzer, R. (2016). Ocean Data View. Retrieved from http://odv.awi.de

Semeniuk, K., & Dastoor, A. (2017). Development of a global ocean mercury model with a methylation cycle: Outstanding issues. *Global Biogeochemical Cycles*, *31*, 400–433. https://doi.org/10.1002/2016GB005452

Shaffer, G. (1986). Phosphate pumps and shuttles in the Black Sea. *Nature*, *321*(6069), 515–517. https://doi.org/10.1038/321515a0

Sharif, A., Monperrus, M., Tessier, E., Bouchet, S., Pinaly, H., Rodriguez-Gonzalez, P., et al. (2014). Fate of mercury species in the coastal plume of the Adour River estuary (Bay of Biscay, SW France). *Science of the Total Environment*, *496*, 701–713. https://doi.org/10.1016/j.scitotenv.2014.06.116

Si, Y., Zou, Y., Liu, X., Si, X., & Mao, J. (2015). Mercury methylation coupled to iron reduction by dissimilatory iron-reducing bacteria. *Chemosphere*, *122*, 206–212. https://doi.org/10.1016/j.chemosphere.2014.11.054

Skyllberg, U. (2008). Competition among thiols and inorganic sulfides and polysulfides for Hg and MeHg in wetland soils and sediments under suboxic conditions: Illumination of controversies and implications for MeHg net production. *Journal of Geophysical Research*, *113*, G00C03. https://doi.org/10.1029/2008JG000745

Slowey, A. J. (2010). Rate of formation and dissolution of mercury sulfide nanoparticles: The dual role of natural organic matter. *Geochimica et Cosmochimica Acta*, *74*(16), 4693–4708. https://doi.org/10.1016/j.gca.2010.05.012

Soerensen, A. L., Jacob, D. J., Schartup, A. T., Fisher, J. A., Lehnherr, I., St. Louis, V. L., et al. (2016). A mass budget for mercury and methylmercury in the Arctic Ocean. *Global Biogeochemical Cycles*, *30*, 560–575. https://doi.org/10.1002/2015GB005280

Soerensen, A. L., Mason, R. P., Balcom, P. H., & Sunderland, E. M. (2013). Drivers of surface ocean mercury concentrations and air–sea exchange in the West Atlantic Ocean. *Environmental Science & Technology*, *47*(14), 7757–7765. https://doi.org/10.1021/es401354q

Soerensen, A. L., Schartup, A. T., Gustafsson, E., Gustafsson, B. G., Undeman, E., & Björn, E. (2016). Eutrophication increases phytoplankton methylmercury concentrations in a coastal sea—A Baltic Sea case study. *Environmental Science & Technology*. https://doi.org/10.1021/acs.est.6b02717

Soetaert, K., & Herman, P. M. J. (2009). A practical guide to ecological modelling: Using R as a simulation platform.
Stanev, E. V., & Kandilarov, R. (2012). Sediment dynamics in the Black Sea: Numerical modelling and remote sensing observations. *Ocean Dynamics*, *62*(4), 533–553. https://doi.org/10.1007/s10236-012-0520-1
Sunderland, E. M., Gobas, F. A. P. C., Branfireun, B. A., & Heyes, A. (2006). Environmental controls on the speciation and distribution of mercury in coastal sediments. *Marine Chemistry*, *102*(1–2), 111–123. https://doi.org/10.1016/j.marchem.2005.09.019
Sunderland, E. M., Krabbenhoft, D. P., Moreau, J. W., Strode, S. A., & Landing, W. M. (2009). Mercury sources, distribution, and bioavailability in the North Pacific Ocean: Insights from data and models. *Global Biogeochemical Cycles*, *23*, GB2010. https://doi.org/10.1029/2008GB003425
Talley, L. D., Pickard, G. L., Emery, W. J., & Swift, J. H. (2011). Physical properties of seawater. In *Descriptive physical oceanography* (pp. 29–65). London: Elsevier.
Tescari, S., Umgiesser, G., Ferrarin, C., & Stanica, A. (2006). Current circulation and sediment transport in the coastal zone in front of the Danube Delta, GEO-ECO-MARINA, 12.
Villemur, R., Lanthier, M., Beaudet, R., & Lépine, F. (2006). The *Desulfitobacterium* genus. *FEMS Microbiology Reviews*, *30*(5), 706–733. https://doi.org/10.1111/j.1574-6976.2006.00029.x
Wang, F., Macdonald, R. W., Armstrong, D. A., & Stern, G. A. (2012). Total and methylated mercury in the Beaufort Sea: The role of local and recent organic remineralization. *Environmental Science & Technology*, *46*(21), 11,821–11,828. https://doi.org/10.1021/es302882d
Wanninkhof, R. (1992). Relationship between wind speed and gas exchange. *Journal of Geophysical Research*, *97*, 7373–7382. https://doi.org/10.1029/92JC00188
Waples, J. S., Nagy, K. L., Aiken, G. R., & Ryan, J. N. (2005). Dissolution of cinnabar (HgS) in the presence of natural organic matter. *Geochimica et Cosmochimica Acta*, *69*(6), 1575–1588. https://doi.org/10.1016/j.gca.2004.09.029
Wesely, M. L. (1989). Parameterization of surface resistances to gaseous dry deposition in regional-scale numerical models. *Atmospheric Environment*, *23*(6), 1293–1304. https://doi.org/10.1016/0004-6981(89)90153-4
Whalin, L., Kim, E.-H., & Mason, R. (2007). Factors influencing the oxidation, reduction, methylation and demethylation of mercury species in coastal waters. *Marine Chemistry*, *107*(3), 278–294. https://doi.org/10.1016/j.marchem.2007.04.002
Woitke, P., Wellmitz, J., Helm, D., Kube, P., Lepom, P., & Litheraty, P. (2003). Analysis and assessment of heavy metal pollution in suspended solids and sediments of the river Danube. *Chemosphere*, *51*(8), 633–642. https://doi.org/10.1016/S0045-6535(03)00217-0
Wool, T. A., Ambrose, R. B., Martin, J. L., & Comer, E. A. (2001). Water Quality Analysis Simulation Program (WASP) Version 6.0: User's Manual.
Yakushev, E. V., Pollehne, F., Jost, G., Kuznetsov, I., Schneider, B., & Umlauf, L. (2007). Analysis of the water column oxic/anoxic interface in the Black and Baltic Seas with a numerical model. *Marine Chemistry*, *107*(3), 388–410. https://doi.org/10.1016/j.marchem.2007.06.003
Yılmaz, A., Çoban-Yıldız, Y., Telli-Karakoç, F., & Bologa, A. (2006). Surface and mid-water sources of organic carbon by photoautotrophic and chemoautotrophic production in the Black Sea. *Deep Sea Research Part II: Topical Studies in Oceanography*, *53*(17–19), 1988–2004. https://doi.org/10.1016/j.dsr2.2006.03.015
Yücel, M., Moore, W. S., Butler, I. B., Boyce, A., & Luther, G. W. (2012). Recent sedimentation in the Black Sea: New insights from radionuclide distributions and sulfur isotopes. *Deep Sea Research Part I: Oceanographic Research Papers*, *66*, 103–113. https://doi.org/10.1016/j.dsr.2012.04.007
Zhang, T., Kim, B., Levard, C., Reinsch, B. C., Lowry, G. V., Deshusses, M. A., & Hsu-Kim, H. (2012). Methylation of mercury by bacteria exposed to dissolved, nanoparticulate, and microparticulate mercuric sulfides. *Environmental Science & Technology*, *46*(13), 6950–6958. https://doi.org/10.1021/es203181m
Zhang, T., Kucharzyk, K. H., Kim, B., Deshusses, M. A., & Hsu-Kim, H. (2014). Net methylation of mercury in estuarine sediment microcosms amended with dissolved, nanoparticulate, and microparticulate mercuric sulfides. *Environmental Science & Technology*, *48*(16), 9133–9141. https://doi.org/10.1021/es500336j
Zhang, Y., Jacob, D. J., Dutkiewicz, S., Amos, H. M., Long, M. S., & Sunderland, E. M. (2015). Biogeochemical drivers of the fate of riverine mercury discharged to the global and Arctic oceans. *Global Biogeochemical Cycles*, *29*, 854–864. https://doi.org/10.1002/2015GB005124
Zhang, Y., Jaeglé, L., & Thompson, L. (2014). Natural biogeochemical cycle of mercury in a global three-dimensional ocean tracer model. *Global Biogeochemical Cycles*, *28*, 553–570. https://doi.org/10.1002/2014GB004814
Zhang, Y., Jaeglé, L., Thompson, L. A., & Streets, D. G. (2014). Six centuries of changing oceanic mercury. *Global Biogeochemical Cycles*, *28*, 1251–1261. https://doi.org/10.1002/2014GB004939